Superconductivity as a probe of anomalous magnetic switching and ferromagnetic stability in Nb/Ni multilayers

Lance De Long, Sergiy Kryukov, Asamoah Bosomtwi, Wentao Xu, E M Gonzalez, E Navarro, J E Villegas, Jose Luis Vicent, Chengtao Yu, Michael J. Pechan

Superconductivity as a probe of anomalous magnetic switching and ferromagnetic stability in Nb/Ni multilayers

Journal:	*Philosophical Magazine & Philosophical Magazine Letters*
Manuscript ID:	TPHM-05-Apr-0106.R1
Journal Selection:	Philosophical Magazine
Date Submitted by the Author:	24-Aug-2005
Complete List of Authors:	De Long, Lance; Univ of Kentucky, Physics and Astronomy Kryukov, Sergiy; University of Kentucky, Physics and Astronomy Bosomtwi, Asamoah; University of Kentucky, Physics and Astronomy Xu, Wentao; University of Kentucky, Physics and Astronomy Gonzalez, E M; Universidad Complutense de Madrid, Departamento de Fisica de Materiales, C C Fisicas Navarro, E; Universidad Complutense de Madrid, Departamento de Fisica de Materiales, C C Fisicas Villegas, J E; Universidad Complutense de Madrid, Departamento de Fisica de Materiales, C C Fisicas Vicent, Jose; Universidad Complutense de Madrid, Departamento de Fisica de Materiales Yu, Chengtao; Miami University, Physics Pechan, Michael J.; Miami University, Physics
Keywords:	magnetic multilayers, magnetometry, superconducting materials, low-dimensional nanomaterials
Keywords (user supplied):	Superconducting multilayers, Magnetic switching

Superconductivity as a probe of magnetic switching and ferromagnetic stability in Nb/Ni multilayers

L. E. DE LONG*, S. A. KRYUKOV*, A. BOSOMTWI*, WENTAO XU*

E. M. GONZALEZ**, E. NAVARRO**, J. E. VILLEGAS**, J. L. VICENT**

CHENGTAO YU† and M. J. PECHAN†

*Department of Physics and Astronomy, University of Kentucky, Lexington, KY 40506-0055 U.S.A.

lander@uky.edu, kryukov@uky.edu, bosomtwi@hotmail.com, wxu2@uky.edu

**Departamento de Fisica de Materiales, C. C. Fisicas, Universidad Complutense, 28040 Madrid, Spain

jlvicent@fis.ucm.es

†Department of Physics, Miami University, Oxford, OH 45056 U.S.A.

yuc@muohio.edu, pechanmj@muohio.edu

Corresponding author: Professor Lance E. De Long, Department of Physics and Astronomy, University of Kentucky, Lexington, KY 40506-0055, U.S.A.

Tel: 1-859-257-4775 FAX: 1-859-323-2846 Email: lander@uky.edu.

The temperature and field dependences of the AC and DC magnetic moment of superconducting and ferromagnetic Nb/Ni multilayers were measured using a SQUID magnetometer with magnetic field applied parallel to the multilayer plane. Periodic kinks in the superconducting upper critical field are evidence for nucleation of a hierarchy of Abrikosov vortex lattices aligned parallel to the multilayer. Small cusps in the low-field, isothermal DC magnetization are evidence that supercurrents are sensitive to extremely small changes in the Ni layer magnetization. Smooth ferromagnetic hysteresis is observed in the normal state, but is supplanted below the superconducting transition by two reproducible discontinuities that indicate magnetic switching of the Ni layers is tightly coupled to the supercurrents. The discontinuities are attributed to the non-dipole character of the moment near switching fields, and therefore cannot be analyzed by standard magnetometer software. Ferromagnetic resonance spectra were measured in parallel and perpendicular DC magnetic fields at room temperature and 4.2 K; and resulting data suggest that Ni layers interact magnetically in the superconducting state.

Keywords: Multilayers, Superconducting thin films, Magnetic switching, Ferromagnetic resonance, Low-dimensional magnetism, SQUID magnetometer

1. Introduction

Ferromagnetic (FM) thin films and multilayers (ML) have been extensively studied and exhibit many interesting properties [**1**]. Finite-temperature phase transitions cannot be realized in ideal two-dimensional systems [**2**], and it is experimentally known that long-range FM order breaks down in favor of "superparamagnetism" if a film is made thin enough [**3**]. In particular, a ML stack of FM thin films interleaved with nonmagnetic layers can be configured as a quasi-two-dimensional system confined along the normal direction to the film plane.

Of course, as the thickness of a magnetic film is decreased, it is increasingly difficult to maintain adequate signal strength from common experimental probes in order to accurately characterize film properties; and this problem is particularly difficult in the case of magnetic moment measurements performed in applied fields parallel to the film plane. Fortunately, the scope of experimental tools is enhanced by superconductivity, which is an established, sensitive probe of magnetic interactions and magnetic moment stability in dilute alloys and compounds [**4**] and more recently, ML [**1**]. Previous studies of bilayers, trilayers and ML have addressed a number of interesting effects of magnetic order on superconducting (SC) properties [**5,6**]. For example, both monotonic [**7**] and nonmonotonic [**8,9**] decreases of the SC transition temperature T_C with FM layer thickness have been observed. These effects have been discussed in terms of the potential roles of pair breaking phase shifts and "π-junctions" [**10**]. FM/SC ML systems may display a variety of other interesting effects, including a number of vortex lattice phase transitions predicted for strongly anisotropic superconductors [**11,12**].

An intriguing competition between FM and SC has been reported for $[Nb(x)/Ni(y)]_Z$ ML [**13,14**]. The sensitivity of superconductivity to Ni layer thickness y appears to depend markedly on the Nb layer thickness x, as shown in **Fig. 1**. The T_C of the ML series with x = 10 nm Nb layers was found to vanish for Ni thickness $y_{CR} \approx 2.5$ nm, above which FM (as detected via Kerr effect) develops for temperatures T ≥ 10 K. The rapid variations of $T_C(y)$ and the Kerr reflectance for the x = 10 nm ML series constitute evidence for the destruction of SC by magnetic fluctuations near a quantum critical point (QCP) located near y_{CR}. On the other hand, $T_C(y)$ was found to be near-constant (with possible small-amplitude oscillations) over a range of Ni thickness 2.5 ≤ y ≤ 6 nm in a second ML series with thicker (x = 23 nm) Nb layers.

We recently discovered that the onset of Nb superconductivity dramatically alters the switching signature of the FM layers in SQUID magnetometer data; and we postulated that screening supercurrents sensitively probe the magnetic stability of the Ni layers [**14**]. The above results have led us to revisit Nb/Ni ML as interesting nanoscale systems whose SC properties might exhibit finite-size, interface and critical fluctuation effects when the FM layer thickness y < 10 nm. A closely related possibility is that the SC condensate interacts with local FM domain wall dynamics generated as Ni layers switch and force large (critical current density $J_C > 10^7$ A/cm^2) Nb supercurrents to redistribute.

Herein, we address these possibilities as part of a review of the temperature and field dependences of the AC and DC magnetic moment of Nb/Ni ML in magnetic fields applied parallel to the film plane, as well as ferromagnetic resonance (FMR) spectra obtained for both parallel and perpendicular field geometries. We also identify and discuss the limitations of using a point-dipole approximation (standard model for the

Quantum Design SQUID Magnetometer) to extract the DC magnetic moment of a SC/FM ML in parallel applied magnetic fields.

2. Experimental details

Ni(y)/[Nb(x=10nm)/Ni(y)]$_8$ and [Nb(x=23nm)/Ni(y)]$_5$ ML with Nb layer thickness x and Ni layer thickness $1.5 \leq y \leq 5$ nm, have been fabricated by DC magnetron sputtering on Si (100) substrates. The samples exhibit textured growth of Nb (110) and Ni (111) layers with negligible interdiffusion and interface roughness [**13,14**]. Samples used in FMR and magnetometer experiments were approximately square with areas in the range 4 x 10^{-6} m^2 to 9 x 10^{-6} m^2. Preliminary electron microscopy (EDAX) investigations reveal that oxygen contamination was not significant during deposition. A typical resistance ratio (room temperature/T_C^+) for a ML sample was 8. Structural data for the sample ML will be discussed in more detail in a separate publication.

We have used a Quantum Design MPMS5 SQUID Magnetometer to measure SC and FM properties of Nb/Ni ML with the applied magnetic field **H** parallel to the ML plane. Field-temperature phase boundaries between SC and normal states were measured using a quasi-static AC magnetic field modulation technique at frequencies $0.1 \leq f \leq 10$ Hz and drive amplitudes $0.01 \leq \mu_o h_o \leq 0.3$ mT. Isothermal magnetization hysteresis curves were obtained using the MPMS5 “Reciprocating Sample Option” (RSO), which optimizes magnetometer sensitivity by executing the low-frequency oscillatory movement of the sample through a superconducting flux-locked loop [**15**].

Most of the RSO data reported herein were acquired using a short (3-cm) scan length and an "Iterative Regression" analysis that permits the sample position to vary in numerical fits of the raw output of the SQUID voltmeter. These methodologies have been generally accepted as useful for improving the reliability of the MPMS5 data analysis software (which assumes the sample is an ideal point dipole [**16**]) in measurements of thin SC films having large demagnetization effects when oriented ***perpendicular*** to the applied magnetic field [**17**]. However, our results show that these data processing procedures fail in situations where macroscopic supercurrents strongly couple to FM domain patterns in SC/FM ML measured in the ***parallel*** geometry.

FMR measurements were carried out at 9.7 GHz in a rectangular cavity in the transverse electric mode (TE_{102}, loaded Q ≈ 5000). Samples were fixed to a rotatable quartz rod by a small amount of vacuum grease so that DC magnetic field could be applied either parallel or perpendicular to the ML plane during measurements. Temperatures down to 4.2 K were attained using a helium gas-flow cryostat. Additional T_C data for FMR samples were acquired via standard AC magnetic susceptibility measurements using a Quantum Design PPMS System operating at f = 10 kHz and amplitude $\mu_o h_o$ = 0.4 mT, with applied DC magnetic fields oriented parallel to the ML plane.

3. Experimental results

3.1. Superconducting phase boundary measurements

Both AC and DC measurements of samples from the $[Nb(23nm)/Ni(y)]_5$ ML series (with y = 2.5, 3.5 or 5 nm) yielded T_C's that were in the range 6.0 to 7.0 K, consistent with previous resistive data [**13,14**] shown in **Fig. 1**. These values are to be compared with $T_C \approx 8.6$ K, 7.0 K and 5.7 K, as observed for single-layer control films of Nb with thickness $t \approx 100$ nm, 20 nm and 10 nm, respectively. These reference values reflect the depression of the transition well below the bulk value of 9.3 K by the effects of finite Nb layer thickness $x << \xi_o \approx 43$ nm [**18**], the coherence length of bulk Nb [**19**].

AC susceptibility data for the $[Nb(23nm)/Ni(y)]_5$ ML set exhibited a nonmonotonic y-dependence of $T_C = 6.88$, 6.98, and 6.00 K, for y = 2.5, 3.5 and 5.0 nm, respectively. A small oscillation of $T_C(y)$ also has been observed in previous resistive measurements of the x = 23 nm ML series for $2.5 \leq y \leq 6.0$ nm [**13,14**], as shown in **Fig. 1**. A nonmonotonic dependence of T_C on the thickness of the FM layer has also been reported in Nb/Gd multilayers [**8**], Fe/V/Fe trilayers [**20**], and Fe/Pb/Fe trilayers [**6**], and has been attributed to pairbreaking associated with an exchange coupling between magnetic layers that oscillates in magnitude and sign as a function of the superconducting layer thickness.

Clear SC transitions could not be observed by AC and DC magnetic measurements above 2 K for the $Ni(y)/[Nb(10nm)/Ni(y)]_8$ set (y = 1.5, 2.5 and 3.5 nm). Results of earlier resistive measurements [**13**] of $[Nb(x)/Ni(y)]_8$ ML ***without an extra Ni capping layer*** are shown in **Fig. 1**. The latter data indicate a strong depression of $T_C \leq 5.3$ K with increasing Ni layer thickness for y > 1.5 nm; and the apparent disagreement with the magnetic data for the capped ML series is not presently understood.

Measurements of the field-temperature phase boundary (upper critical magnetic field $H_{C2}(T)$) yield information concerning the fundamental length scales governing the SC state and the character of any coupling between the Nb layers in the presence of the FM Ni layers [**1**]. In particular, estimates of the coherence length $\xi(T)$ and evidence for two-dimensionality can be obtained from $H_{C2}(T)$ data, where we have assumed that the onset of superconductivity is marked by an abrupt increase in the imaginary part (m'') of the AC magnetic moment in field-cooling experiments. The initial diamagnetic change of the real part (m') of the AC moment can also be used to define an alternative phase boundary, but the m' curve may lie slightly lower (of order 10^{-2} T_C) in temperature than the m'' data in cases of strong pinning of magnetic flux [**21**,**22**].

The low-field portion of the m''(H,T) boundary does not exhibit deviations from three-dimensional (linear) behavior [**1**], except possibly very close to T_C, as shown in the inset to **Fig. 2a**. We have considered a simplified picture of a two-dimensional SC layer of thickness x between two FM layers with zero SC order parameter at the interfaces, as discussed by Jin and Ketterson [**1**], who give the following relation (gaussian units) for the zero-temperature value of H_{C2}:

$$H_{C2}(0) = (5.53)\Phi_o/2\pi\xi_o x \qquad \textbf{(1)}$$

Estimating $H_{C2}(0) \approx 3.5 \times 10^4$ Oe from **Fig. 2** and the Nb layer thickness x = 23 nm, we obtain a zero-temperature coherence length $\xi_o \approx 23$ nm = x, which is at the borderline between two- and three-dimensional behavior for a single Nb layer. Alternatively, a simple, three-dimensional Ginzberg-Landau model analogous to **Eq. 1** yields

$$H_{C2}(0) = \Phi_o/2\pi\xi_o^2 \qquad \textbf{(2)}$$

The latter relation gives $\xi_o \approx 9.8$ nm << x, which is consistent with three-dimensional behavior.

Electron scattering can have significant effects on the behavior of $H_{C2}(T)$, and can be roughly estimated from **Eq. 2** by replacing ξ_o^2 by $\xi_o l_{tr}$, which is valid in the "dirty limit" (transport mean-free path $l_{tr} < \xi_o$ [**23**]) with DC field applied perpendicular to the ML [**1**]. For example, resistivity data [**24**] for a $[Nb(10nm)/Ni(1.5nm)]_8$ ML yield a transport mean-free path $l_{tr} \approx 4.3$ nm parallel to the Nb planes (assuming a free-electron model with one conduction electron per Nb [**25**], and that the conductivity of the thinner Ni layers is negligible). Perpendicular upper critical field data [**13**] then yield $\xi_o \approx 40$ nm, close to the value for bulk Nb [**19**], and consistent with the dirty limit approach.

Close examination of the m"(H,T) boundary reveals weak "kinks" below T_C, and these anomalies persist to fields of at least 0.65 T with an average period $\mu_o \delta H \approx 73.3$ mT, as shown in **Fig. 2**. Periodic extrema ("matching anomalies") in the critical current, magnetization and $H_{C2}(T)$ of SC materials can be observed at applied fields where the average density of flux lines (FL) is equal to an integral multiple of the pinning center density. Matching anomalies are relatively well defined in the case of thin films and ML if the FL pinning centers are located on a periodic lattice and have a characteristic size $\xi(T) < D < \lambda(T)$ [**21**,**22**]. The only apparent periodic structure capable of pinning FL in the present case is the ML repeat unit (see **Fig. 3a**), which leads to the supposition that such effects are a consequence of the confinement of quantized FL to the cross-sectional area of individual Nb layers in the parallel field geometry.

A simple approach to explain the kinks is to assume that a number N_L FL enter a single Nb layer in successive chains [**26-28**] that form along the perpendicular edge of length L (≈ 3 mm for the y = 5 nm sample) when the ML is oriented parallel to the applied field **H**. A schematic arrangement of the FL in an isolated Nb plane is shown in **Fig. 3b**. It is important to note that the thickness of a single Nb layer is w = x = 23 nm < λ_o ≈ 43 nm [**19**], the zero-temperature penetration depth of clean, bulk Nb. If the SC order parameter = 0 in the Ni layers (total confinement of supercurrents within a Nb plane) we must assume that the FL cross-sections are approximately elliptical with major and minor axes of length $\lambda_{||}$ and w, respectively, where $\lambda_{||}$ represents the penetration depth parallel to the ML. The condition for flux quantization and the known ML parameters then yield $(\delta H)wL \approx N_L\Phi_o$ and $2N_L\lambda_{||} \approx L$, and imply $N_L \approx 2.4 \times 10^3$ and $\lambda_{||} \approx$ 614 nm (Φ_o is the flux quantum). We use these results and a relation $\pi w\lambda_{||} \equiv \pi\lambda_I^2$ to extract an "effective" isotropic penetration depth λ_I ≈ 84 nm ≈ $2\lambda_o$, where the rough factor of 2 could easily be accounted for by finite mean-free-path and two-dimensional confinement effects [**29**]. Since N_L >> 1, and the ML were not precisely aligned with the applied DC field, neither do we expect the FL chains to be perfectly ordered, nor the matching anomalies to be perfectly periodic in applied field. This crude model therefore yields a plausible explanation of the phase boundary kinks.

However, noting that x < ξ_o ≈ 30 - 40 nm for $[Nb(10nm)/Ni(y)]_8$ ML [**13**] and clean, bulk Nb [**19**], one must consider the possibility that the Nb layers are proximity-coupled via the Ni layers (of thickness y << ξ_o). Specifically, if the superconducting order parameter is nonzero in the Ni layers, the presumed "chain" of FL should re-distribute among the coupled Nb and Ni layers available (i.e. the assumed SC layer spans the ***entire***

ML cross-section, and Ni layers present periodic FL pinning sites). A corresponding estimate that assumes that one row of N_L cylindrical FL enters the ML cross section of total width w = 140 nm (five repeat units of a Nb(x = 23 nm)/Ni(y = 5 nm) bilayer) yields $\lambda = 101$ nm $\approx (2.4)\lambda_o$.

Note that the values of $\lambda >> x$ generated by the last set of estimates support a scenario in which supercurrents flow between Nb layers via a finite SC order parameter within the Ni layers. This scenario is also consistent with the relatively small value x = 23 nm of the Nb layer thickness compared to the bulk Nb FL core size $\approx 2\xi_o \approx 80$ nm, and the existence of oscillations of $T_C(y)$ generated by pairbreaking within the Ni layers, as shown in **Fig. 1**. Moreover, these characteristic lengths are all well below the total thickness (140 nm) of the $[Nb(23nm)/Ni(5nm)]_5$ ML, and are therefore consistent with the linear, three-dimensional behavior observed in the m" phase boundary shown in **Fig. 2**.

However, magnetic pairbreaking, proximity effects and interface scattering also must be taken into account in a quantitative model of SC/FM ML data [**1**]. In the absence of a rigorous microscopic theory for the Nb/Ni ML case, we must extract estimates of characteristic length scales that govern the interlayer couplings by investigation of additional physical properties.

3.2 Magnetic moment measurements

The "standard" manifestation of flux matching in patterned SC thin films in perpendicular magnetic fields is observation of sharp cusp or peak anomalies in the isothermal magnetization curves [**21**,**22**]. Alternatively, in the more relevant situation where field was applied parallel to SC planes, peaks have been observed in the m(H) curves of SC/normal-metal ML [**26**], SC/FM ML [**30**,**31**] and high-T_C [**31-33**] superconductors. Although these anomalies were attributed to flux matching effects, the observed peaks were separated by relatively large field intervals of 10^{-2} to 1 T, were not precisely periodic in field, and were often a mix of narrow and broad features.

In the present case of $[Nb(23nm)/Ni(y)]_5$ ML, we observed small cusp anomalies in the field dependence of the SC state magnetic moment m(H) (see **Figs. 4a** and **4b**) near H = 0; whereas we have observed only smooth FM hysteresis in the normal state for fields applied parallel to the ML plane and fixed temperatures just above $T_C \approx 5.8$ K, as shown in **Fig. 5**. It is apparent that the rough spacing between the cusps in **Figs. 4a** and **4b** is not strongly affected by changes in temperature just below T_C, as expected for a flux matching effect that is mainly dependent on the arrangement and density of pinning centers. On the other hand, the strong temperature dependences (very close to $T_C \approx 6$ K) of the coherence length $\xi(T)$ and penetration depth $\lambda(T)$ will affect the FL pinning strength and electromagnetic coupling between Ni layers, respectively. For example, smearing (without changing the spacing) of matching anomalies by random pinning forces generally strengthens with decreasing temperature and higher FL density [**21**,**22**]. Such an effect may be evident in **Fig. 5a**, where the small cusp and abrupt switching anomalies are absent in an initial magnetization loop measured well below T_C at T = 3.5 K. However, increasing T to just below T_C (**Fig. 5c**), or changing the magnetic history (e.g., “training” on successive field cycling) of the sample (**Fig. 5b**) results in the appearance of the cusps. Furthermore, the smooth FM reversal observed in the normal state hysteresis curves is replaced by a remarkable effect below T_C, where two symmetric, ***highly reproducible*** (on repeated field cycling) jumps of the diamagnetic signal occur near or above the FM coercive fields, which suggests that they mark a sudden switching of the Ni magnetization. Another interesting feature is the "latching" of m(H) at exactly zero at the midpoints of the switching anomalies, as shown in **Fig. 5b** (also see **Fig. 6**, below).

The proposed QCP (defined by a critical Ni layer thickness $y_{CR} \approx 2.5$ nm, at which superconductivity and FM order simultaneously decrease toward T = 0, as shown in **Fig. 1**) is presumably caused by the instability of long-range FM order in $[Nb(10nm)/Ni(y)]_8$ ML with Ni layer thickness y ≤ 2.5 nm [**14**]. Therefore, strong effects of temperature and finite Ni layer thickness on the magnetization data also might be expected for the other series of $[Nb(23nm)/Ni(y)]_5$ ML with y ≈ 2.5 nm, as shown in **Fig. 6**. Indeed, the initial magnetization curve (**Fig. 6a**) of the $[Nb(23nm)/Ni(2.5nm)]_5$ ML exhibits strong discontinuities for $\mu_o|H| > 50$ mT at T = 5.0 K. These apparently "random instabilities" are absent (even in the initial magnetization) at a lower temperature T = 3.5 K (as shown in **Fig. 6b**), consistent with a rapidly increasing stability of the FM state with decreasing temperature in this temperature and composition regime.

The effects of training and interactions between supercurrents and the FM layers are also exibited by the $[Nb(23nm)/Ni(2.5nm)]_5$ ML at a slightly ***higher*** temperature T = 5.5 K, as shown in **Fig. 7a**. These data exhibit anomalies for $\mu_o|H| > 30$ mT as emphasized in **Fig. 7b**, where we have subtracted the normal state FM hysteresis curve (which is essentially temperature-independent near T_C) from the SC state data. The difference curve emphasizes the contribution of supercurrents to the sample magnetization. The initial linear magnetization curve (blue line) is consistent with a Meissner diamagnetic response that is followed by entry into the mixed state, accompanied by a number of anomalies that could be generated by random flux avalanche events [**34**]. Finally, there is an abrupt collapse of the inferred SC response near $\mu_o H = 35$ mT. However, further field cycling generates two ***highly symmetric*** groups of magnetization anomalies near ±35 mT, and sharp collapses of the supercurrent magnetization shown in **Fig. 7b** near ±50 mT. Note that the unstable field interval at T = 5.5 K shown in **Fig. 7** is consistent with that observed at T = 5 K, as shown in **Fig. 6a**.

Additional experiments were conducted to determine if the stability of the Ni magnetization is strongly dependent on Ni layer thickness near y ≥ 2.5 nm, and temperatures in the range 4 – 10 K. Magnetic moment data at T = 5.0 K for a sample with a slightly thicker Ni layers (y = 3.5 nm) are shown in **Fig. 8**. Moment discontinuities are absent in these data, which is consistent with a comparatively high stability of the FM state for y = 3.5 nm under these measuring conditions.

The apparent change in character of the magnetization curves upon cooling into the SC state can be interpreted as evidence for a close coupling between the supercurrent response of the SC condensate and the FM switching of the Ni layers. We have speculated that the highly reproducible, discontinuous jumps in m(H) might be due to "supercurrent-induced" switching of the Ni moments [**14**]. Crude estimates of the current density J_C necessary to account for the SC state magnetization near zero field in **Fig. 5** yield values as high as 10^8 to 10^9 A/cm^2, depending upon the value of penetration depth chosen.

We also have argued that the SC condensate within Nb/Ni ML acts as a "current amplifier" of the Ni moments and their fluctuations [**14**]. This line of reasoning assumes that the cusp anomalies evident in **Figs. 4a** and **4b** are due to abrupt rearrangements of the FL lattice driven by subtle (i.e., hard to detect in normal state data) FM domain wall motion or local magnetization dynamics, as have been observed in sensitive vibrating reed measurements on bulk FM superconductors [**35**]. Such magnetic anomalies are difficult to observe in the normal state of FM materials, where they are responsible for "Barkhausen noise" [**36**].

However, it is important to keep in mind that interpretations of the SC state moment data depend upon the quantitative reliability of the software fitting routines applied to the raw MPMS5 SQUID voltmeter output. Surprisingly, we have found that the compelling reproducibility and symmetry of the sharp anomalies shown in **Figs. 5-8** ***does not even guarantee their qualitative validity***, as discussed below.

3.3 Caveats Concerning SQUID Magnetometer Data

It is widely known that SQUID magnetometer data processing software can yield erroneous results when SC samples having large demagnetization coefficients (thin plates and films are oriented perpendicular to the applied magnetic field) [**17**]. In these cases, small magnetic field gradients caused by imperfections and flux trapping in the magnetometer SC solenoid can alter the magnetic response of the sample, which no longer behaves as a stable point-dipole. The effects of non-uniform field can be largely avoided by minimizing the distance the sample travels ("scan length") during each measurement, and executing procedures that eliminate trapped flux in the SC solenoid [**15-17**].

Nevertheless, we have encountered a novel effect that complicates the evaluation of MPMS SQUID Magnetometer data for FM thin film and ML samples oriented ***parallel*** to the applied field. This is normally a situation in which large demagnetization effects and nonuniform applied fields are not expected to be serious problems. On the other hand, the magnetization of a FM layer of finite length aligned parallel to the applied magnetic field will generally be composed of domains of variable size and orientation that form a mosaic of magnetic dipoles, as opposed to the single point-dipole assumed by the MPMS Magnetometer software. This situation generally results in the movement of the apparent sample position ("center") as the domain structure reverses and rearranges in variable temperature and field environments. The Quantum Design MPMS Magnetometer software offers the "Iterative Regression" option, which treats the sample position as a fit variable in the evaluation of the SQUID voltmeter output. It is therefore tempting to use the Iterative Regression option to improve fit quality in cases where the sample does not move, but the magnetization does distort during FM reversal. As long as the FM layer can be approximated by a dominant single domain of a size that is much smaller than the separation (1.5 cm) between SQUID sense coils, satisfactory fits of RSO data can be obtained, which is apparently the case for the "fully trained", normal-FM-state response of Nb/Ni ML, as reflected in **Figs. 5** and **9**.

We have regularly monitored the "regression fit" parameter R that assesses the quality of fit of the SQUID voltmeter output that is converted into a calibrated magnetic moment datum. We have determined that values of R > 0.90 are typical for the normal-

FM-state hysteresis data (see **Fig. 9**), indicating that the Ni layers behave very consistent with the MPMS5 software requirement that the sample be a single, point-magnetic-dipole. Excursions (greater than the sample size!) in the fitted sample position are, however, apparent in the initial (virgin) magnetization of the $[Nb(23nm)/Ni(5nm)]_5$ ML at T = 6.0 K (see **Figs. 5c** and **9**); and this behavior cannot be simply dismissed as due to a FM domain distribution that is not yet "well trained".

The indicators of fit quality change more dramatically in the SC state (see **Fig. 10**), where unphysically large movement of the sample position apparently occurred over a wide range of applied field. Brief summaries of the behavior of the R parameter are given in the figure captions to help the reader assess the reliability of the fitted data. We emphasize that the SC state moment data were ***extremely reproducible*** once the two switching anomalies were established in the initial magnetization cycle, and the MPMS software yielded satisfactory fits (which we arbitrarily define by $R \geq 0.80$) except for narrow field intervals surrounding the abrupt switching anomalies (see **Fig. 10**).

Alternatively, use of the standard "Linear Regression" option of the MPMS software, which assumes a fixed geometrical sample position, will yield inferior fit quality (R) in measurements of finite-sized FM ML in the parallel field geometry. One manifestation of such a failure is the "latching" of the Nb/Ni ML moment at zero in the middle of an abrupt switch in the SC state, as shown in **Figs. 5** and **6**. When the best-fit sample position varies by more than 1 cm, the MPMS software automatically replaces the Iterative Regression with the Linear Regression procedure [**17**] which, in the present case, returns a default, zero moment and quality of fit R = 0, as shown in **Fig. 10**. Moreover, none of the standard MPMS Magnetometer software options are quantitatively reliable at DC fields near the apparent switching anomalies, which is also evident in **Fig. 10**.

Even though the standard MPMS5 software may not be appropriate for quantitative processing of the raw input data from the SQUID voltmeter under experimental conditions where the point-dipole model fails, the SQUID voltmeter signal remains a reliable measure of the sample's magnetic response, and is not dependent upon which fitting procedure is adopted to process the raw voltmeter output [**16,17**]. Indeed, the remarkable reproducibility of the fitted MPMS5 RSO data strongly suggests that once a well defined pattern of FM domains is established within the Ni layers, a corresponding, unique supercurrent response that is tightly coupled to the Ni magnetization is also established. The reproducibility of the magnitude of abrupt changes in the fitted output and the fields at which they occur also rules out simple, random FL avalanche events as a probable mechanism for such anomalies. Specialized techniques (valid for a particular sample geometry and magnetic behavior) can be developed for a quantitative evaluation of the SQUID voltmeter output observed for Nb/Ni ML; and our recent success in developing a novel fitting routine for the data of **Figs. 5-8** will be described in a separate publication.

3.4 Ferromagnetic Resonance Results

Ferromagnetic resonance (FMR) is a powerful probe of the FM properties of ML and thin films, including magnetic moment, magneto-elastic coupling coefficients, and magnetic anisotropy [**37**,**38**]. In spite of the extensive research on the physical properties of

FM/SC ML, FMR has not been widely applied to these systems. We are interested in FMR characterization of Nb/Ni ML since the magnetic coupling between FM Ni layers and the boundary conditions appropriate to FMR in Nb/Ni ML may be affected by a transition to a SC state (that may, or may not be localized within the Nb spacer layers); and this situation could be further modified by a nonzero SC order parameter and screening in thin FM Ni layers, or a magnetic polarization induced within the SC layers.

Fig. 11 shows FMR absorption derivative of three Ni(y)/[Nb(10 nm)/Ni(y)]$_8$ samples at room temperature and 4 K for DC magnetic field applied in the ML plane. The FMR spectra change markedly with the Ni layer thickness y; in particular, the resonance amplitude of the uniform mode increases much more rapidly than linearly with y for samples that all had comparable planar area. The trends in resonance amplitude are not, therefore, due to the relative amount of Ni present in the samples. The strongest peak (presumed to be the uniform mode [**39**]) was down-shifted by 39.0, 32.4, and 20.7 mT (field at the absorption peak for y = 1.5, 2.5, and 3.5 nm, respectively) when measured at 4 K, compared to the room-temperature value. Since the x = 10 nm ML series samples were not superconducting, these shifts cannot be attributed to field inhomogeneities or screening by supercurrents, and probably reflect a temperature dependence in the FM state of the Ni layers.

The FMR spectra of the same Ni(y)/[Nb(10 nm)/Ni(y)]$_8$ samples with DC magnetic field applied perpendicular to the ML plane are more complex, as shown in **Fig. 12**; and the field scale of the observed modes is roughly twice that of the parallel field case shown in **Fig. 11**. A single (which we assume is either a broadened uniform mode or two crossing modes) resonance signature appears for Ni layer thickness y = 2.5 nm**.** At least two modes are observed for samples with y = 1.5 and 3.5 nm. The sample with y = 3.5 nm exhibits at least one resonance (at 452.5 mT) below the uniform mode (518.7 mT) at RT, whereas two resonances (at 395.3 and 505.4 mT) appear below the uniform mode (611.2 mT) at 4 K. The broadening and changes in amplitude of the resonances again suggest that the FM state is temperature dependent between room temperature and 4 K.

The FMR modes of the second $[Nb(23nm)/Ni(y)]_5$ ML series of samples have relatively weak amplitude and therefore details of complex spectra, if present, could not be detected. Note that the resonance amplitude decreases with decreasing Ni layer thickness y; and no FMR signal could be detected for either applied field orientation for the smallest Ni layer thickness y = 2.5 nm. Only the uniform mode is observed for y = 3.5 and 5 nm with DC magnetic field applied either parallel or perpendicular to the sample plane, as shown in **Figs. 13** and **14**. This suggests that the interlayer coupling is very weak and each Ni layer resonates independently in the same mode. Although the samples are superconducting below 6 K at zero magnetic field, they may not remain superconducting at the fields applied during the FMR measurements. In particular, there is no big difference between the RT and 4 K spectra in **Fig. 14**, which were taken at perpendicular applied fields above 0.1 T, where the ML are expected to be in the normal FM state at 4 K, based upon perpendicular $H_{C2}(T)$ data not shown here. On the other hand, the 4 K data for the parallel field orientation (**Fig. 13**) are slightly shifted and broadened compared to the room temperature data, as expected if magnetic induction gradients due to the shape anisotropy of the superconducting magnetization are present.

4. Discussion

4.1 Superconducting and ferromagnetic phase boundaries

First, it is important to note that our magnetometer data do not yield any evidence for superparamagnetic behavior in the normal state for any Ni layer thickness studied, which implies that at least some type of short-range FM order is present, as opposed to an ideal "quantum critical" case in which no long-range FM order should be present at finite temperatures near a QCP. The Kerr effect data of **Fig. 1**, which suggest there is no FM order below 10 K for Ni layer thicknesses $y < 2.5$ nm, might be better explained by a systematic reduction in the size of well-ordered Ni domains with decreasing y to a value comparable to, or below, the wavelength of the probe radiation (of order 100 nm). Of course, this scenario also implies that the Ni domains are both small and not well aligned for $y \approx 2.5$ nm. Using data for the spontaneous moment (0.604 Bohr magnetons) of bulk Ni [**40**] and the approximate dimensions of the $[Nb(23nm)/Ni(5nm)]_5$ ML (square sample of side $L = 2.5 \times 10^{-3}$ m), we calculate an in-plane Ni moment = 8.05×10^{-5} emu for the normal FM state, which is in very good agreement with the data in **Fig. 6c**. Precise data for the y-dependence of the volume-scaled saturation magnetization in the normal state would be useful in assessing the stability of the FM state of the Ni layers.

Second, the $Ni(y)/[Nb(x)/Ni(y)]_8$ ML set studied herein exhibited no clear evidence of superconductivity at temperatures above 2.2 K, whereas previous resistive data [**13**] for a different set of $[Nb(10nm)/Ni(y)]_8$ ML yielded a dramatic decrease of T_C from 5.3 K for $y \approx 0$ to well below 2 K for $y \geq 2.2$ nm, as shown in **Fig. 1**. A possibly crucial difference is that the SC samples possessed an even number (8) of both Ni and Nb layers, but stacked in an asymmetric manner (one Nb layer on the Si substrate was not covered by a Ni layer); whereas the Ni(y)/[Nb(10nm)/Ni(y)]$_8$ ML set newly investigated in the present study had an odd number (9) of Ni layers with a even number (8) of Nb layers that were all bounded by two Ni layers.

In contrast, the [Nb(23nm)/Ni(y)]$_5$ samples, which were taken from the same batch of ML for both the present and previous studies [**13**,**14**], have an odd number of Ni layers and an odd number of Nb layers. The latter ML set exhibits robust superconductivity over a range of temperatures below 7 K, and the data from AC and DC magnetization and electrical resistance measurements of T_C are in good agreement. The behavior of the ML series with x = 23 nm make it unlikely (but not impossible) that an unintentional mishap in sample preparation is responsible for the different behaviors of the two ML series with x = 10 nm, but having different configurations of Ni capping layers.

Further research should address the possibility that the combined actions of the SC proximity effect and magnetic pairbreaking interactions within the Ni layers lead to phase shifts or changes in boundary conditions governing the SC condensate wavefunction that are sensitive to the presence of an additional Ni capping layer between the Si substrate and the first Nb layer. Such a possibility could provide interesting explanations for a number of aspects of our results.

4.2 Coupling between superconducting and ferromagnetic layers

The finite thickness of both the Ni and Nb layers could influence the coupling between the SC and FM order parameters via quasiparticle or pair tunneling. The supercurrent density within Nb layers in the critical state is expected to be at least 10^6 or 10^7 A/cm^2 [**41**], which is large enough (consider a tunneling supercurrent bridging adjacent Nb layers through the intervening Ni layer) to initiate the abrupt switching of the Ni via a "spin torque" mechanism [**42**,**43**]. The abrupt switching anomalies in **Figs. 5-8** are at least superficial evidence for such an effect. However, we caution that the standard MPMS5 Magnetometer fits of the SC state data are not quantitatively valid near these switching anomalies.

Another important consideration is how differences in (even/odd) number of Ni layers could lead to significant changes in the electromagnetic coupling between different Ni layers and the occurrence of "flux closure" states among pairs of oppositely magnetized Ni layers, especially for applied magnetic fields near zero. The "latching" of the magnetization at precisely zero at the midpoint of the switching anomalies observed for the ML series with x = 23 nm is indicative of such a flux closure state, assuming that the magnetization of an odd Ni layer is exactly screened by the Nb layers. However, the output of the MPMS5 SQUID voltmeter is severely distorted from that expected for a single point-dipole near the latching points; and these special points correspond to fields at which the MPMS Magnetometer fitting procedure fails completely (R = 0).

In spite of the ambiguities introduced by the occasional failure of the MPMS5 data analysis software, the data in **Figs. 4-8** provide clear evidence for the sensitivity of the SC condensate to small changes in the Ni magnetization. Furthermore, these data provide excellent illustrations of the strong synergy between the reversal of the Ni moments and the SC magnetic response (compare the large magnitude of the SC magnetic moment with the normal state FM moment, as well as a strong shift of the SC state switching field to well above the normal state coercive field in **Fig. 6**, for example).

4.3 Flux matching effects in the superconducting state

The cusp and kink anomalies in the magnetization and SC-normal phase boundary data are evidence for "flux matching", and there are several models that could be relevant to our results. For example, the geometry of a SC/FM ML of rectangular cross-section subjected to a parallel magnetic field (as in **Fig. 3a**) meets the general conditions for the "terraced critical state" proposed by Cooley and Grishin [**44**]. Specifically, they assumed a rectangular superconducting slab whose plane was parallel to an external applied field; but the slab was also assumed to have a periodic array of strong pinning centers that were shown to lead to periodic, "saw tooth" anomalies in the DC magnetic moment as a function of parallel magnetic field.

Another type of matching effect has been predicted [**27**] and observed [**28**] in highly anisotropic bulk superconductors and ML [**26**] when FL enter a sample in successive chains that extend along the length of crystal planes oriented approximately parallel to the applied field **H**. Indeed, the rough spacing of the cusps shown in **Fig. 4** is 1.5-3.0 mT, and they extend to approximately ± 8.0 mT, which is similar to the matching field scale in thin films patterned with antidot lattices [**21**,**22**]. The asymmetry of the magnetization curve near H = 0 could be due to the Bean-Livingston penetration barrier [**45**] that acts against vortex penetration, but not against vortex removal. We note the existence of very subtle variations of the magnetic moment (on the field-decreasing sides of H = 0) having a rough periodicity comparable to the cusps in **Fig. 4**; but we do not discuss these features since they are not sufficiently defined above the scatter in the data.

On the other hand, the spacing of the cusps in the isothermal m(H) data is not uniform and is very different from the kink spacing in the AC phase boundary shown in **Fig. 2b**. The irregular spacing of the cusps in field sweep data could be due to a strong and inhomogeneous vortex pinning landscape [**21**,**22**] that generates a nonequilibrium "critical state" [**29**], whereas the larger spacing of kinks in the phase boundary of **Fig. 2b** is determined by AC experiments with DC field-cooling, which would involve a different degree of equilibration. Calculations [**26**,**46**,**47**] predict that a succession of FL lattices will form as vortices penetrate a single, thin film superconductor in an increasing parallel field; but these phases will have different packing topologies whose ranges of stability may not be strictly periodic in applied field. This situation is at least qualitatively consistent with the anomalies shown in **Fig. 4**.

A novel, alternative explanation of the cusp anomalies in m(H) originates from a primary motivation of this investigation: We hoped to discover evidence that the superconducting state can amplify very small changes in the Ni layer magnetization and sensitively reflect details of the interactions between the Ni and Nb layers at the ML interfaces. The small jumps in the m(H) data of **Fig. 4** could be due to an amplified SC response to small rearrangements of Ni domain walls or local magnetic reversals within Ni layers. Ordinarily, the microscopic dynamics of the FM state are extremely small, and are relegated to Barkhausen noise or tiny "stick-slip" events that make up the fine structure of the normal FM hysteresis curves. The nearly reproducible patterns of these jumps apparent in **Fig. 4** would then point to a remarkably reproducible sequence of domain wall motion and growth patterns during the magnetic reversal of the Ni layers. It remains to unambiguously identify mechanisms governing the influence of the proximate SC Nb layers on the symmetry and near periodicity of the cusps in m(H) shown in **Fig. 4**.

4.4 Ferromagnetic resonance

The microscopic mechanism of a particular FMR resonance mode is not obvious in the absence of micromagnetic simulation results for ML. In the case of FM permalloy dot lattices, “hybrid” FMR modes that arise from both exchange and dipolar interactions between spins have been reported [**48**]. Spin wave resonances with finite wavevector $k > 0$ are hard to observe in very thin films (< 10 nm), and the field separation between the modes should be much larger than observed here [**38**]. Ajan et al. reported that three-dimensional coupling between FM layers exists in Nb/Co ML with Nb layer thickness up to 13.5 nm [**49**]. Therefore, 2D and 3D layer couplings may be possible in the Nb/Ni ML having Nb layer thickness $x \approx 10$ nm.

Nevertheless, information concerning the stability of the FM state is apparent from the FMR data. The lack of FMR signal for the $[Nb(23nm)/Ni(2.5nm)]_5$ ML is consistent with the expectation generated by **Fig. 1** that this sample may have relatively unstable FM order or a fine-grain domain structure that reduces the FMR response at room temperature or 4 K. The magnetization data of **Figs. 6** and **7** are consistent with the presence of FM domain instabilities at temperatures close to the SC T_C. The stabilization of the magnetization signal at temperatures well below T_C is also consistent with an enhancement of long-range FM order, or simply the growth of more ordered, larger domains at lower temperature. The weak amplitude and slight broadening of the FMR spectra at 4K for the $[Nb(23nm)/Ni(y)]_5$ ML with y = 3.5 and 5.0 nm are consistent with inhomogeneities of magnetic induction in the SC state.

It is useful to compare the rather weak room temperature FMR data for the $[Nb(23nm)/Ni(y)]_5$ ML series to the corresponding data for the $Ni(y)/[Nb(10nm)/Ni(y)]_8$ ML series. The comparison suggests that interactions between Ni layers are stronger for the x = 10 nm ML, and these "three-dimensional" interactions help stabilize the FM state and yield the relatively strong FMR signals shown in **Figs. 11** and **12**. The fact that the FMR resonances actually strengthen for the $Ni(1.5nm)/[Nb(10nm)/Ni(1.5nm)]_8$ sample at 4 K, and do not dramatically change with temperature for the other two samples with thicker Ni layers, is consistent with the absence of superconductivity and the increased FM stability of the x = 10 nm ML compared to the x = 23 nm series. We also reiterate that the small differences in sample area and the number of Ni layers cannot explain the observed differences in FMR signal between the x = 10 and 23 nm ML series.

Summary and conclusions

The stability of the FM state of two series of [Nb(x)/Ni(y)] ML was studied using FMR with applied DC magnetic field parallel and perpendicular to the sample plane at room temperature and 4 K. We observed a strong dependence of the FMR spectra on the thickness of both Ni and Nb layers, and weak shifts in the resonance fields and modest line broadening were observed when the ML were superconducting. Our results suggest that various degrees of three-dimensional magnetic interactions exist in Nb/Ni ML, depending upon the thickness of Ni and Nb layers, and whether or not the Nb layers are superconducting. Detailed analyses of these data using micromagnetic simulation techniques will be required to help sort out the contributions of "hybrid" dipole and exchange couplings [**48**] to the FMR response and their effect on the coupling between Ni layers.

AC measurements of the approximate field-temperature phase boundaries for the SC state revealed three-dimensional behavior and weak kink anomalies in $H_{C2}(T)$ for DC fields applied parallel to the ML plane; and FL pinning or transitions between FL lattice phases are mechanisms consistent with the near-periodic spacing (of order 0.1 T) of the kinks. It is possible that the deposition of two (as opposed to one) Ni capping layers strongly suppresses the T_C of the Ni(y)/[Nb(10nm)/Ni(y)]$_8$ ML.

Measurements of the SC magnetization in parallel applied fields near zero revealed small cusp anomalies spaced by field intervals of 1 - 3 mT. Although the cusps were not exactly periodic in field, they were approximately reproducible on field cycling, and were prominent when field was increasing in magnitude after crossing H = 0, suggesting they are due to very subtle changes in the domain structure of the FM Ni layers that are amplified by the supercurrent response.

The parallel magnetization of the SC state exhibited two symmetric, abrupt jumps at, or well beyond (depending upon the Ni layer thickness y), the coercive magnetic fields seen in the normal FM state. These jumps were extremely reproducible after no more than one field cycle, and often exhibited "latching" of the sample moment at exactly zero over a very small field interval at the midpoint of a jump (making it appear to be a two-step process). Moreover, these data suggest that the magnetic reversal of the Ni layers is strongly coupled to the supercurrent response of the Nb layers via long-range dipolar and/or shorter-range "spin torque" mechanisms that could provide a novel means of controlling the magnetic switching of a FM layer. However, the failure of the MPMS5 SQUID Magnetometer software to fit SC state moment data near the jumps prevents a clear interpretation of these anomalies.

Ongoing, extensive examinations of a large body of SC state data taken with the Quantum Design MPMS5 SQUID Magnetometer under different field-temperature histories and employing novel data fitting procedures have revealed a subtle, reproducible magnetic reversal process coupled to the supercurrent response that we will discuss in more detail in a separate publication.

Acknowledgments

Research at University of Kentucky supported by U.S. DoE Grant #DE-FG02-97ER45653. Research at Universidad Complutense supported by Spanish CICY Grant #MAT02-04543 and ESF VORTEX Program. Research at Miami University was supported by U.S. DoE Grant #DE-FG02-86ER45281.

References

[1] B. Y. Jin and J. B. Ketterson, Advances in Physics **38** 189 (1989).

[2] N. D. Mermin and H. Wagner, Phys. Rev. Lett. **17** 1133 (1966).

[3] A. P. Kuprin, L. Cheng, D. W.Lee, Z. Altounian and D. H. Ryan, J. Appl. Phys. **85** 5738 (1999).

[4] M. B. Maple, Physica B **215** 110 (1995).

[5] F. Y. Ogrin, S. L. Lee, A. D. Hillier, A. Mitchell, and T. H. Shen, Phys. Rev. B **62** 6021 (2000).

[6] L. Lazar, K. Westerholt, H. Zabel, L. R. Tagirov, Yu. V. Goryunov, N. N. Garif'yanov, and I. A. Garifullin, Phys. Rev. B **61** 3711 (2000).

[7] J. Aarts, J. M. E. Geers, E. Brück, A. A. Golubov, and R. Coehoorn, Phys. Rev. B **56** 2779 (1997).

[8] J. S. Jiang, D. Davidovic, D. H. Reich, and C. L. Chien, Phys. Rev. Lett. **74**, 314 (1995).

[9] M. Velez, M. C. Cyrille, S. Kim, J. L. Vicent, and Ivan K. Schuller, , Phys. Rev. B **59** 14659 (1999).

[10] Z. Radovic, M. Ledvij, L. Dobrosavljevic-Grujic, A. I. Buzdin, and J. R. Clem, Phys. Rev. B **44** 759 (1991).

[11] A. Buzdin and A. Yu. Simonov, Physica C **167** 388 (1990).

[12] A. I. Buzdin, S. S. Krotov and D. A. Kuptsov, Physica C **175** 42 (1991).

[13] J. E. Villegas, E. Navarro, D. Jaque, E. M. Gonzalez, J. I. Martín, and J. L. Vicent, Physica C **369** 213 (2002).

[14] S. A. Kryukov, L. E. De Long, E. Navarro, J. E. Villegas, E. M. Gonzalez and J. L. Vicent, IEEE Trans. Magnetics **39** 2693 (2003).

[15] *MPMS Reciprocating Sample Option Documentation Package* (Quantum Design Publication No. 1090-101, San Diego, CA, 1996).

[16] M. McElfresh, *Fundamentals of Magnetism and Magnetic Measurements* (Quantum Design, San Diego, CA, 1994).

[17] M. McElfresh, Shi Li and R. Sager, *Effects of Magnetic Field Uniformity on the Measurement of Superconducting Samples* (Quantum Design, San Diego, CA, 1996).

[18] I. Banerjee, Q. S. Yang, C. M. Falco and I. K. Schuller, Solid State Communications **41** 805 (1982).

[19] D. K. Finnemore, T. F. Stromberg and C. A. Swenson, Phys. Rev. **149** 231 (1966).

[20] L. R. Tagirov, I. A. Garifullin, N. N Garif'yanov, S. Ya. Khlebnikov, D. A. Tikhonov, K. Westerholt and H. Zabel, J. Magn. Magn. Matt. **240**, 577 (2002).

[21] L. E. De Long, S. Lokhre, T. Yun, V. V. Metlushko, V. V. Moshchalkov and Y. Bruynseraede, Physica C **369** 118 (2002).

[22] V. V. Metlushko, L. E. De Long, M. Baert, E. Rosseel, M. J. Van Bael, K. Temst, V. V. Moshchalkov and Y. Bruynseraede, Europhys. Lett. **41** 333 (1998).

[23] T. P. Orlando, E. J. McNiff, Jr., S. Foner and M. R. Beasley, Phys. Rev. B **19** 4545 (1979).

[24] E. Navarro, J. E. Villegas and J. L. Vicent, J. Magn. Magn. Mat. **240** 586 (2002).

[25] V. R. Karasik and I. Yu. Shebalin, Sov. Phys.: JETP **30** 1068 (1970).

[26] S.-W. Han, J. Farmer, P. F. Miceli, G. Felcher, R. Goyette, G. T. Kiehne and J. B. Ketterson, Physica B **336** 162 (2003).

[27] A. I. Buzdin and A. Yu. Simonov, Physica C **175** 143 (1991).

[28] C. A. Bolle, P. L. Gammel, D. G. Grier, C. A. Murray, D. J. Bishop, D. B. Mitzi and A. Kapitulnik, Phys. Rev. Lett. **66** 112 (1991).

[29] M. Tinkham, *Introduction to Superconductivity* (McGraw-Hill, New York, 1975), Chapt. 4.

[30] S. H. Brongersma, E. Verweij, N. J. Koeman, D. G. de Groot, R. Griessen and B. I. Ivlev, Phys. Rev. Lett. **71** 2319 (1993).

[31] M. Ziese, P. Esquinazi, P. Wagner, H. Adrian, S. H. Brongersma and R. Griessen, Phys. Rev. B **53** 8658 (1996).

[32] C. Hünnekes, H. G. Bohn, W. Schilling and H. Schulz, Phys. Rev. Lett. **72** 2271 (1994).

[33] A. A. Zhukov, G. K. Perkins, Y. V. Bugoslavsky and A. D. Caplin, Physica C **282-287** 2223 (1997).

[34] F. L. Barkov, D. V. Shantsev, T. H. Johansen, P. E. Goa, W. N. Kang, H. J. Kim, E. M. Choi and S. I. Lee, Phys. Rev. B **67** 064513 (2003).

[35] L. De Long, J. Childers, A. Olinger, Jr., Q. Chen, J.-C. Hou, U. Lahaise, J. Zhang, D. G. Hinks, P. Canfield, R. Schweinfurth, D. Van Harlingen, and M. Norton, Physica B **223&224** 22 (1996)

[36]. P. Mazzetti, A. Stepanescu, P. Tura, A. Masoero and I. Puica, Phys. Rev. **B** 65 132512 (2002).

[37] B. Heinrich and J. F. Cochran, Adv. Phys. **42** 523 (1993).

[38] M. Farle, Rep. Prog. Phys. **61** 755 (1998).

[39] C. Kittel, Phys. Rev. **11** 1295 (1958).

[40] D. H. Martin, *Magnetism in Solids* (MIT Press, Cambridge, MA, 1967).

[41] A. Terentiev, B. Watkins, L. E. De Long, L. D. Cooley, D. J. Morgan and J. B. Ketterson, Physica C **332** 5 (2000).

[42] J. A. Katine, F. J. Albert, R. A. Buhrman, E. B. Myers and D. C. Ralph, Phys. Rev. Lett. **84** 3149 (2000).

[43] S. Urazhdin, N. O. Birge, W. P. Pratt, Jr. and J. Bass, Phys. Rev. Lett. **91** 146803 (2003).

[44] L. D. Cooley and A. M. Grishin, Phys. Rev. Lett. **74** 2788 (1995).

[45] C. P. Bean and J. D. Livingston, Phys. Rev. Lett. **12** 14 (1964).

[46] L. S. Levitov, Phys. Rev. Lett. **66** 224 (1991).

[47] C. C. de Souza Silva, L. R. E. Cabral and J. Albino Aguiar, Physica C **404** 11 (2004).

[48] S. Jung, B. Watkins, L. De Long, J. B. Ketterson and V. Chandrasekhar, Phys. Rev. B **66** 132401 (2002).

[49] A. Ajan, S. Prasad, R. Krishnan, N. Venkataramani, and M. Tessier, J. Appl. Phys. **91** 1444 (2002).

Figure Captions

Fig. 1. Superconducting transition temperature $T_C(y)$ (left vertical axis) for $[Nb(10nm)/Ni(y)]_8$ (open symbols) and $[Nb(23nm)/Ni(y)]_5$ (solid symbols) ML series as functions of Ni layer thickness y (horizontal axis). Fractional change in reflectivity $\delta_{kerr} = \Delta R_{kerr}/R$ (right vertical axis) of the magneto-optical Kerr effect signal (at saturation) at temperature T = 10 K for the series with 10 nm Nb layers. After [**14**].

Fig. 2a. Magnetic field - temperature phase boundary between the superconducting and normal states for a $[Nb(23nm)/Ni(5nm)]_5$ ML, as measured by the onset temperature of an abrupt increase in the imaginary part m" of the AC magnetic moment. Data were taken in field-cooling experiments at AC frequency f = 10 Hz and amplitude $\mu_o h_o = 0.05$ mT with applied DC field H parallel to the ML plane. Inset shows an enlarged view of the low-field regime.

Fig. 2b. Superconducting field - temperature phase boundary data of **Fig. 2a**, emphasizing the region just below the zero-field T_C. Arrows denote "kinks" that are proposed as roughly periodic "matching anomalies" in the phase boundary (see text for discussion).

Fig. 3a. Schematic cross-section (not drawn to scale) of a $[Nb(x)/Ni(y)]_5$ ML in an external magnetic field **H** oriented parallel to the ML plane. The black field denotes the Si substrate, the gray fields the superconducting Nb layers, and the white fields the ferromagnetic Ni layers. Note the absence of a Ni capping layer between the Si substrate and the first Nb layer.

Fig. 3b. Schematic diagram of FL confinement in one Nb layer (length L and width w) of a Nb/Ni ML. The applied field **H** is oriented parallel to the ML plane and perpendicular to the layer side of length L. The diagram depicts an artificially small number N_L = 3 FL forming a "chain" within the Nb layer. Assuming the SC order parameter is zero in neighboring FM Ni layers, confinement of the supercurrents within the Nb layer demands that FL have elliptical cross-section (white field with crosses) with major and minor axes of length $\lambda_{\parallel}$ and w, respectively.

Fig. 4a. DC magnetic moment m versus magnetic field H applied parallel to the $[Nb(23nm)/Ni(5nm)]_5$ ML held at a temperature T = 3.8 K. Arrows denote rough positions of cusps that may signal a flux matching effect. These data are re-plotted from the low-field regions of the isothermal (T = 3.8 K) magnetization curve shown in **Fig. 5b**. Note the cut in the vertical axis.

Fig. 4b. DC magnetic moment m versus magnetic field H applied parallel to the $[Nb(23nm)/Ni(5nm)]_5$ ML held at a temperature T = 5.0 K. Arrows denote rough positions of cusps that may signal a flux matching effect. These data are re-plotted from the low-field regions of the isothermal (T = 5.0 K) magnetization curve shown in **Fig. 5c**. Note the cut in the vertical axis.

Fig. 5a. DC magnetic moment m versus magnetic field H applied parallel to a $[Nb(23nm)/Ni(5nm)]_5$ ML for temperatures T = 6.0 K (normal FM state, black curve) and T = 3.5 K (SC state, red points). Normal state data were taken after the sample was initially degaussed at T = 250 K, then zero-field cooled to T = 6 K for field-cycling. The quality of fit for the nearly all of the normal FM state data exceeds 0.85 (see **Fig. 9**). The SC state data were obtained for the sample initially at $\mu_o H = 0.1$ T and T = 4.0 K after a previous field cycle; the sample was then field-cooled to 3.5 K and field-cycled from H = 0. The quality of fit R > 0.80 for SC state data for $\mu_o|H| < 20$ mT (excepting the initial magnetization data for the Meissner state).

Fig. 5b. DC magnetic moment m versus magnetic field H applied parallel to a $[Nb(23nm)/Ni(5nm)]_5$ ML for temperatures T = 6.0 K (normal FM state, black curve) and T = 3.8 K (below T_C, red points). The normal FM state data are the same for **Figs. 5a**, **5b** and **5c**. The dashed lines denote two symmetric switching anomalies located near ± 20 mT in the SC state. The quality of fit R > 0.80 for SC state data everywhere except over narrow intervals of width ≈ 5 mT about the switching anomalies. The SC state data were taken in a manner similar to those of **Fig. 6c**; and an expanded view of the data near H = 0 is given in **Fig. 4a**.

Fig. 5c. DC magnetic moment m versus magnetic field H applied parallel to a $[Nb(23nm)/Ni(5nm)]_5$ ML for temperatures T = 6.0 K (normal FM state, black curve) and T = 5.0 K (below T_C, red points). Dashed lines denote two symmetric switching anomalies near $\mu_o H = \pm 20$ mT in the SC state data, which were taken after the sample was degaussed at T = 250 K, then field-cooled in 50 mT to T = 5 K for field cycling from $\mu_o H = 0$ T. R > 0.80 for SC state data (see **Fig. 10**) everywhere except for intervals of width ≈ 4 mT about the switching anomalies. An expanded view of the SC state data near H = 0 is given in **Fig. 4b**.

Fig. 6a. DC magnetic moment m versus magnetic field H applied parallel to a $[Nb(23nm)/Ni(2.5nm)]_5$ ML for temperatures T = 6.5 K (normal FM state, black curve) and T = 5.0 K (below T_C, red points). The normal state fit quality R > 0.90 except for a narrow interval of around 2 mT about the coercive fields. SC state data were obtained after the sample was degaussed at T = 250 K, then field-cooled in 50 mT to T = 5 K, whereupon H was set to 0, and the sample field-cycled. Abrupt switching anomalies in the SC state are located near ± 0.11 T, where R < 0.80 (for $-0.14 \text{ T} \leq \mu_o H \leq 0.09$ T and $0.1 \text{ T} \leq \mu_o H \leq 0.13$ T).

Fig. 6b. DC magnetic moment m versus magnetic field H applied parallel to a $[Nb(23nm)/Ni(2.5nm)]_5$ ML for temperatures T = 6.5 K (normal FM state, black curve) and T = 3.5 K (below T_C, red points). The dashed lines denote two symmetric switching anomalies located near ± 0.16 T, which are clearly displaced from the normal FM coercive fields observed at 6.5 K. The quality of fit R for the SC state data was in the range 0.75 < R < 0.85 for |H| < 0.15 T, and 0.64 < R < 0.80 for |H| > 0.15 T. The SC state data were taken after previous field cycling (see **Fig. 6a** for comparison).

Fig. 7a. DC magnetic moment m versus magnetic field H applied parallel to a $[Nb(23nm)/Ni(2.5nm)]_5$ ML for temperatures T = 8.5 K (normal FM state, black curve) and T = 5.5 K (below T_C, red points). The quality of fit R > 0.90 for the normal state FM data, except for fields within intervals of approximate width = 2 mT about the coercive fields. SC state data were obtained after the sample was field-cooled from 10 K in $\mu_o H$ = 50 mT, and then field cycled from H = 0. R > 0.80 for SC state data for $|\mu_o H|$ > 50 mT, but dropped rapidly below 0.60 within intervals of approximate width = 60 mT about the switching anomalies. During an initial magnetization from 0 to 0.3 T, irreproducible anomalies set in near $\mu_o H$ = + 20 mT, and precede full reversal of the magnetization at higher applied fields.

Fig. 7b. Plot of the difference between the DC magnetic moment m of **Fig. 7a** in the SC state (T = 5.5 K) and the normal state (T = 8.5 K). Blue points were taken in the initial magnetization sweep from 0 to 0.3 T, and red points were measured upon further field cycling. Note the bands of reproducible anomalies located beyond ± 30 mT that precede reversal of the magnetization at higher applied fields. The initial linear section of the blue trace behaves like a Meissner state, then exhibits an abrupt collapse near 35 mT, after which it is indistinguishable from the normal FM state data.

Fig. 8. DC magnetic moment m versus magnetic field H applied parallel to a $[Nb(23nm)/Ni(3.5nm)]_5$ ML for temperatures T = 6.5 K (normal state above T_C, black points) and T = 5.0 K (below T_C, red points). The blue trace denotes the initial (virgin) magnetization curve that begins in the SC Meissner state. The quality of fit R > 0.99 for normal state data everywhere except at the coercive fields. Sample was degaussed at T = 250 K, then field-cooled in 50 mT to 5K, and field-cycled from H = 0. The quality of fit

R > 0.78 for SC state data everywhere except for intervals of approximate width = 20 mT about the switching anomalies, and the initial magnetization branch. Note the nonmonotonic behavior preceding the switching anomalies at $\pm$ 60 mT.

Fig. 9. Fit quality R (left axis, red and black curves) and Center Offset (right axis, blue curve) from fits of the SQUID voltmeter data versus applied magnetic field H parallel to a $[Nb(23nm)/Ni(5nm)]_5$ ML at temperature T = 6.0 K (normal FM state). The red (black) curve is for field decreasing (increasing). A plot of the corresponding magnetic moment data is shown in **Fig. 5**.

Fig. 10. Fit quality R (left axis, red and black curves) and Center Offset (right axis, blue curve) from fits of the SQUID voltmeter data versus applied magnetic field H parallel to a $[Nb(23nm)/Ni(5nm)]_5$ ML at temperature T = 5.0 K (SC state). The red (black) curve is for field decreasing (increasing). A plot of the corresponding magnetic moment data is shown in **Fig. 5c**.

Fig. 11. FMR absorption derivative versus applied magnetic field applied parallel to $Ni(y)/[Nb(10\ nm)/Ni(y)]_8$ sample plane for different Ni layer thickness y = 1.5 **(a)**, 2.5 **(b)**, and 3.5 nm **(c)**. Dashed and solid curves correspond to room temperature and 4 K, respectively.

Fig. 12. FMR absorption derivative for applied DC magnetic field perpendicular to $Ni(y)/[Nb(10\ nm)/Ni(y)]_8$ sample plane for different Ni layer thickness y = 1.5 **(a)**, 2.5

(b), and 3.5 nm **(c)**. Dashed and solid curves correspond to room temperature and 4 K, respectively.

Fig. 13. FMR absorption derivative measured with DC magnetic field parallel to [Nb(23 nm)/Ni(y)]$_5$ sample plane for different Ni layer thickness y = 3.5 **(a)** and 5.0 nm **(b)**. Dashed and solid curves correspond to room temperature and 4 K, respectively. No resonance was observed for the sample with y = 2.5 nm.

Fig. 14. FMR absorption derivative measured with DC magnetic field perpendicular to [Nb(23 nm)/Ni(y)]$_5$ sample plane for different Ni layer thickness y = 3.5 **(a)** and 5.0 nm **(b)**. Dashed and solid curves correspond to room temperature and 4 K, respectively. No resonance was observed for the sample with y = 2.5 nm.

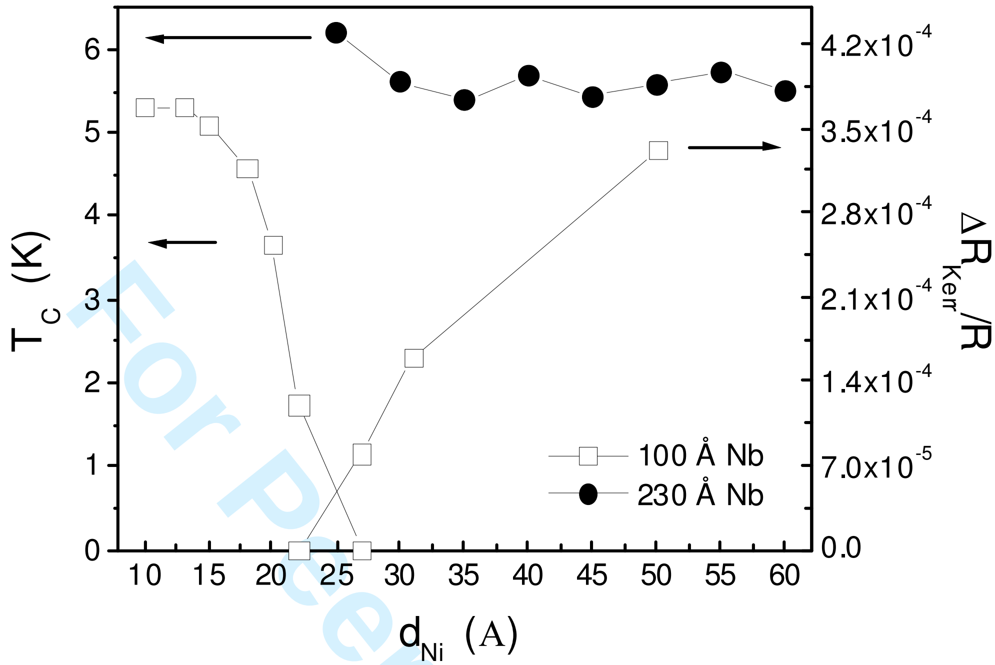

Fig. 1 De Long et al.

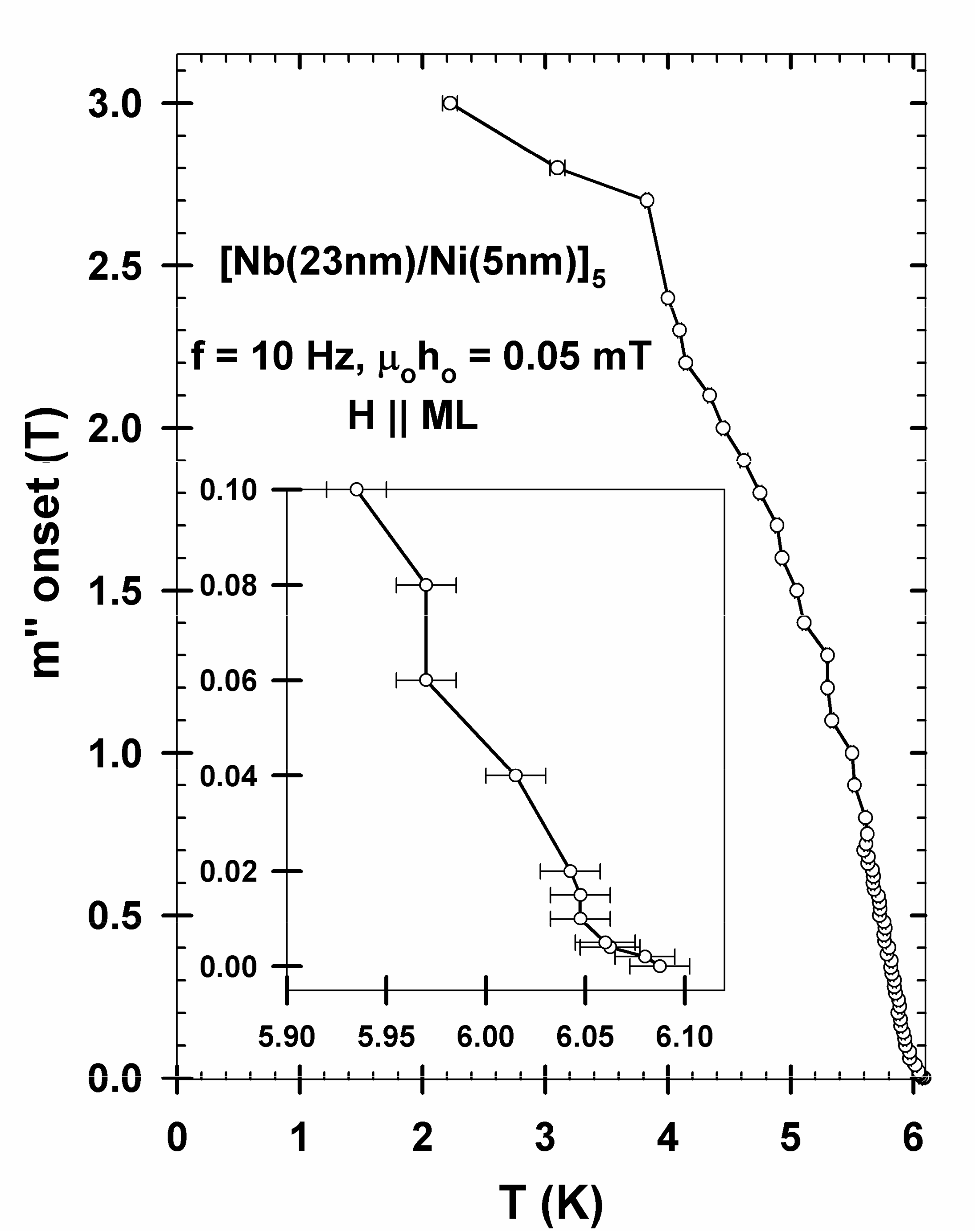

Fig. 2a De Long et al.

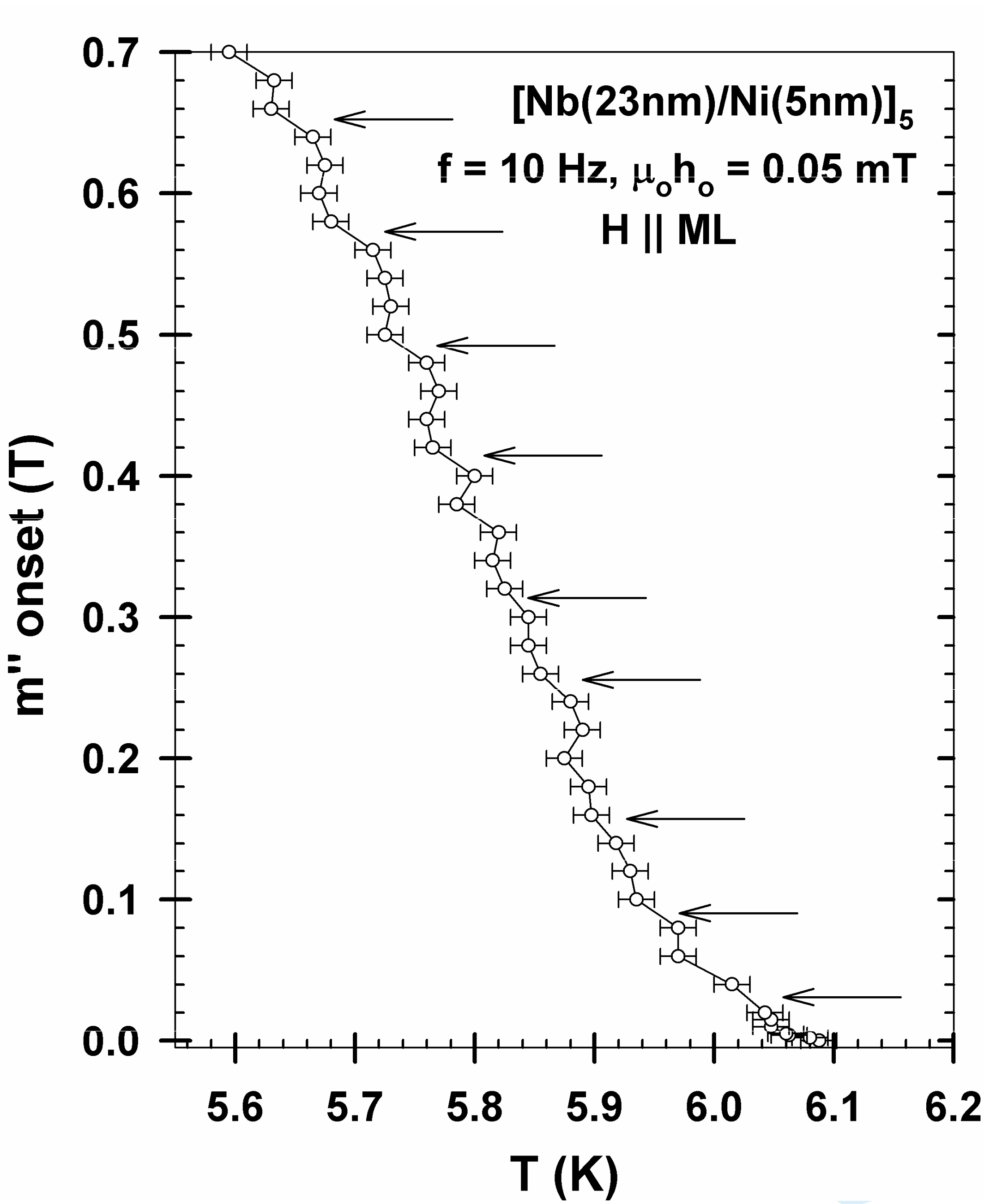

Fig. 2b De Long et al.

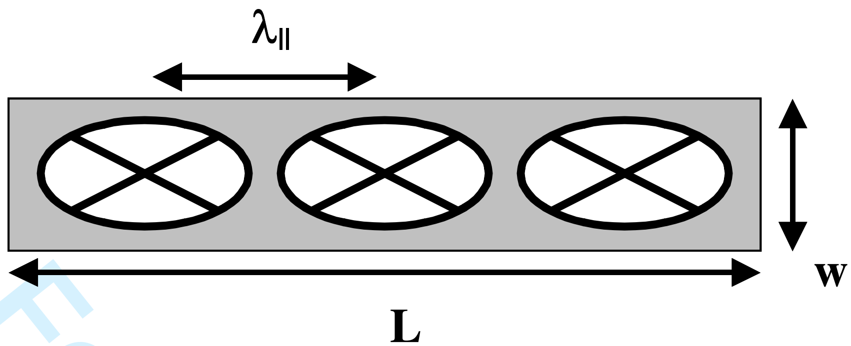

Fig. 3b De Long et al.

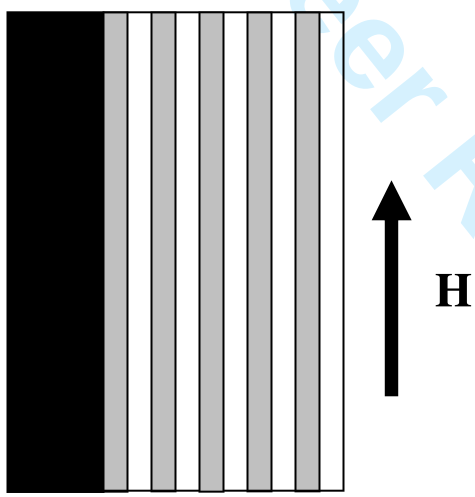

Fig. 3a De Long et al.

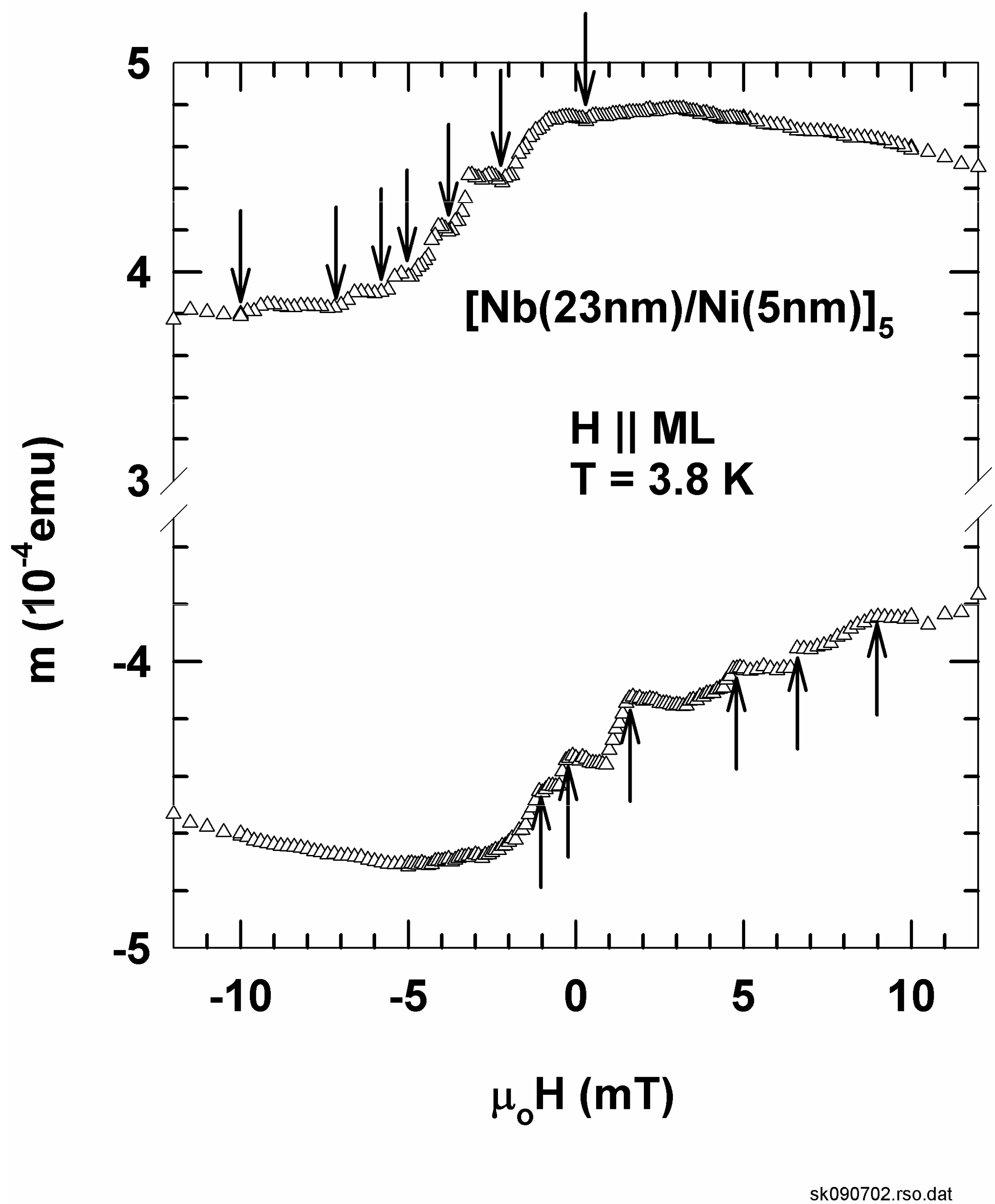

Fig. 4a De Long et al.

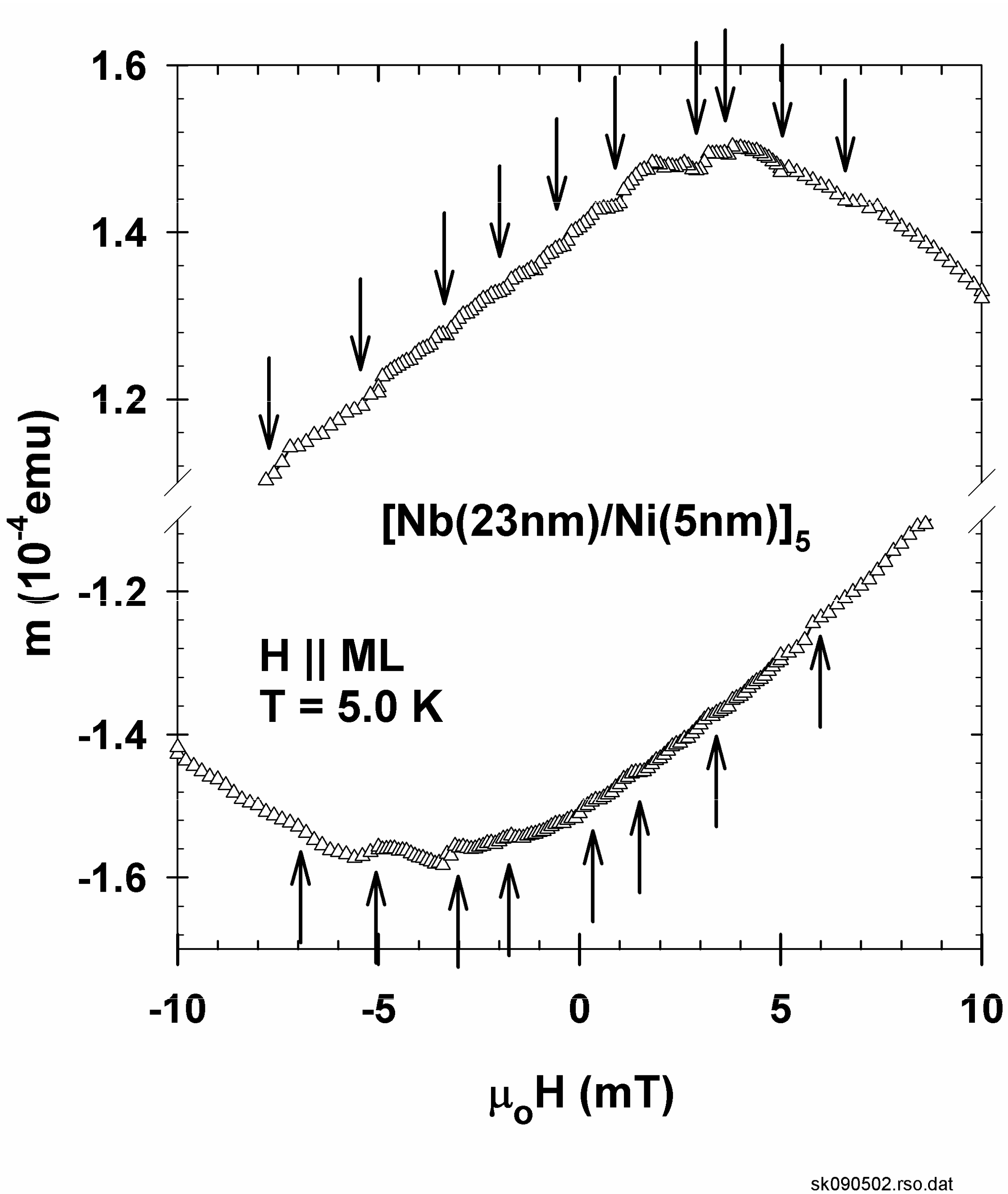

Fig. 4b De Long et al.

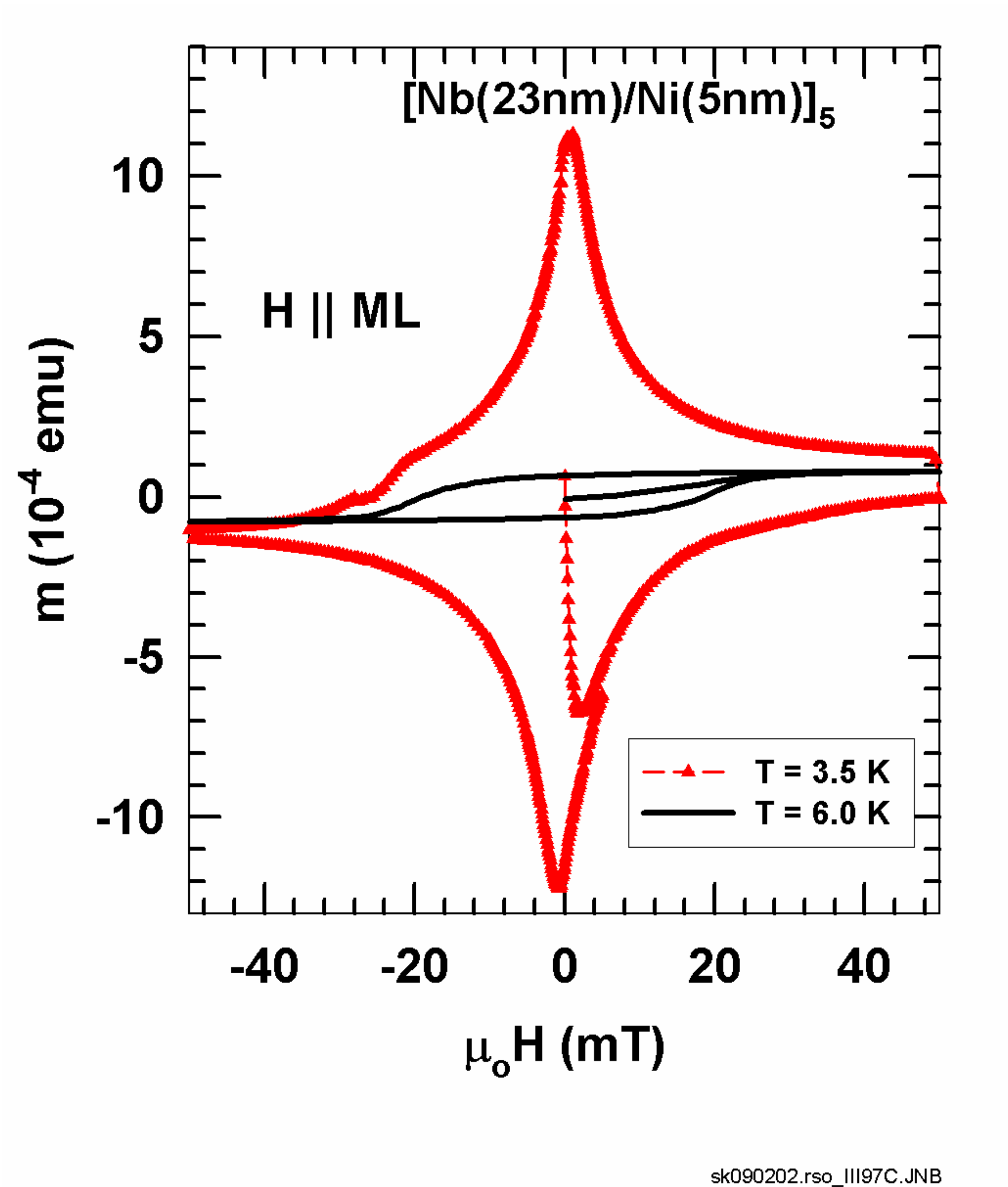

Fig. 5a De Long et al.

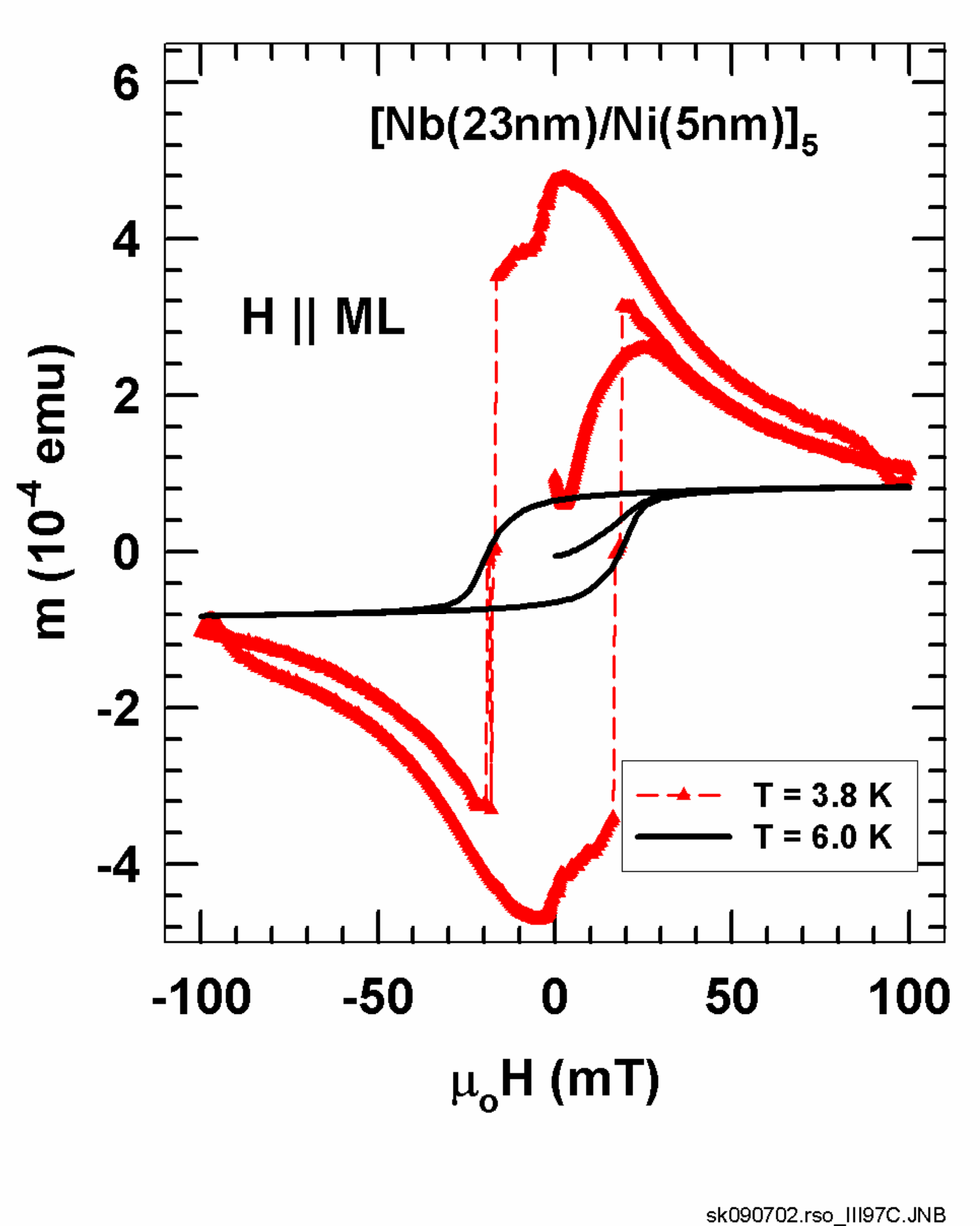

Fig. 5b De Long et al.

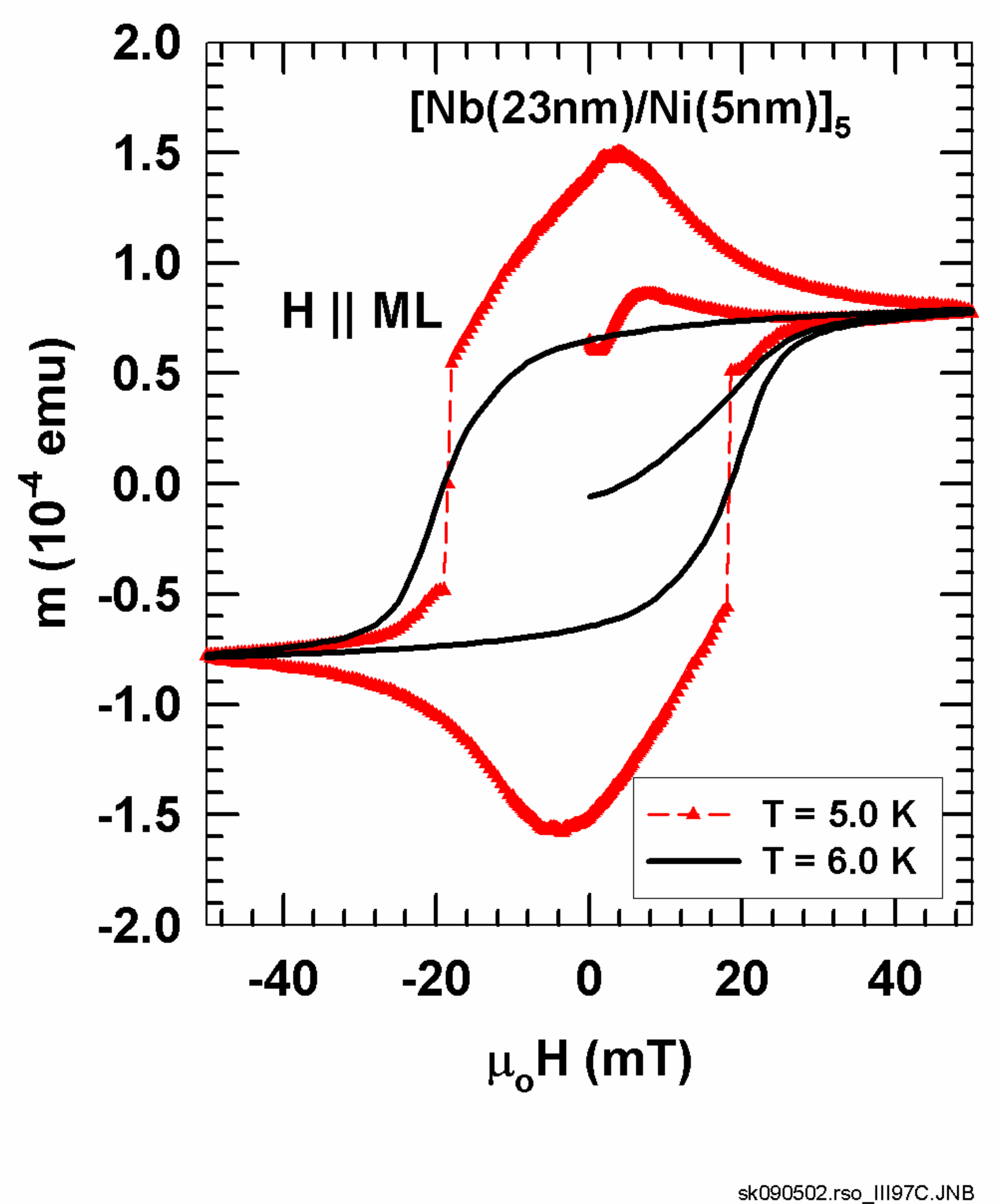

Fig. 5c De Long et al.

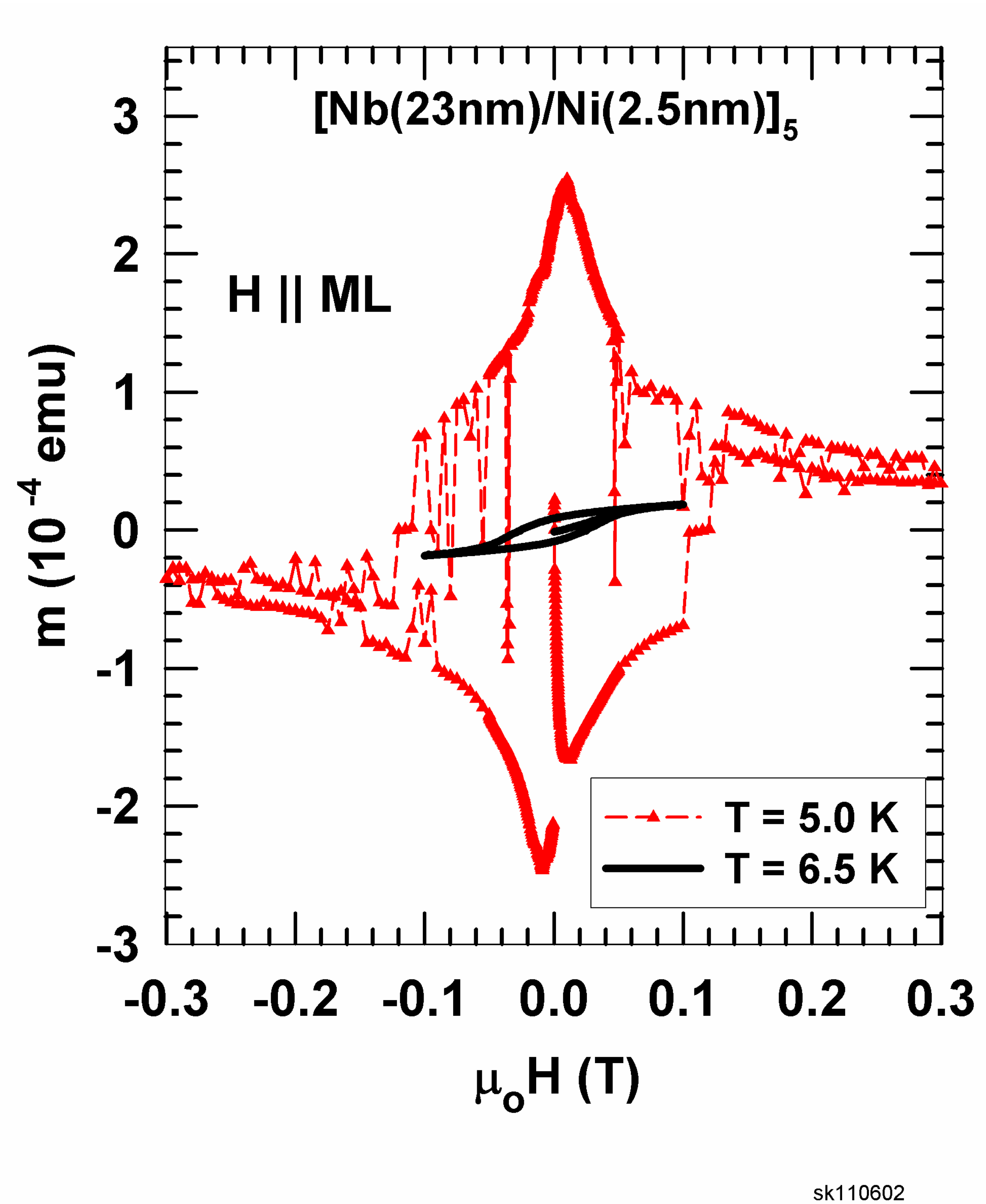

Fig. 6a De Long et al.

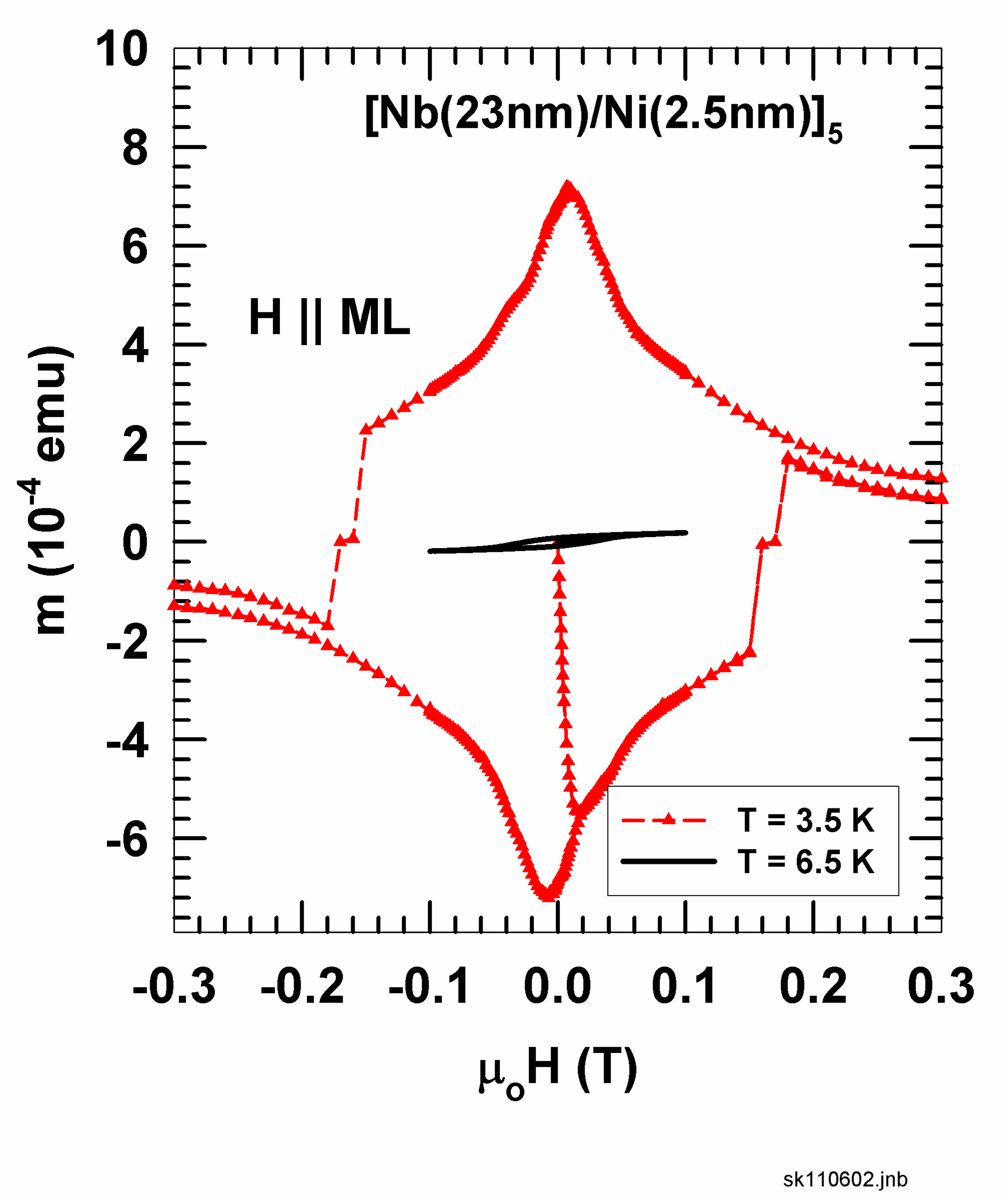

Fig. 6b De Long et al.

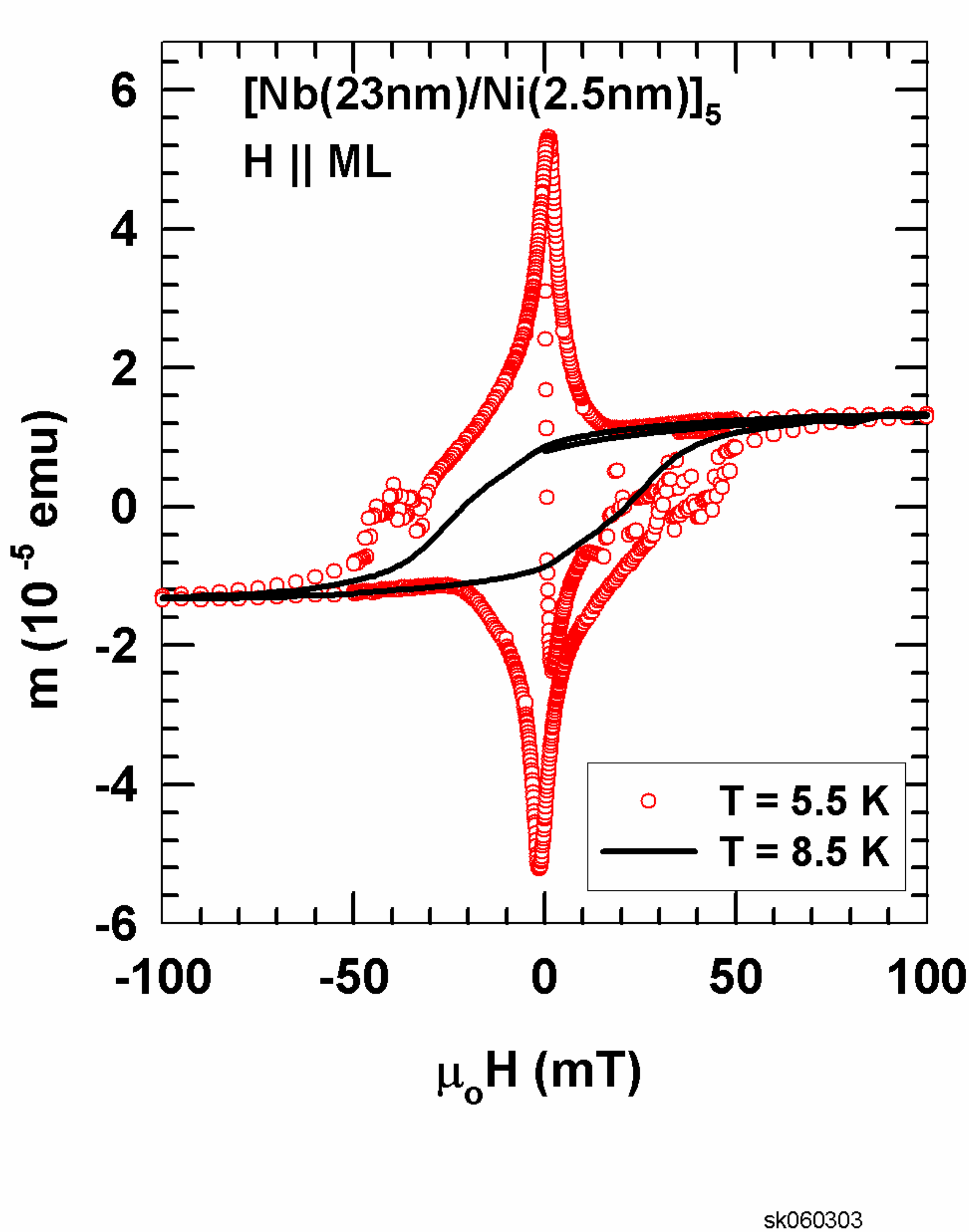

Fig. 7a De Long et al.

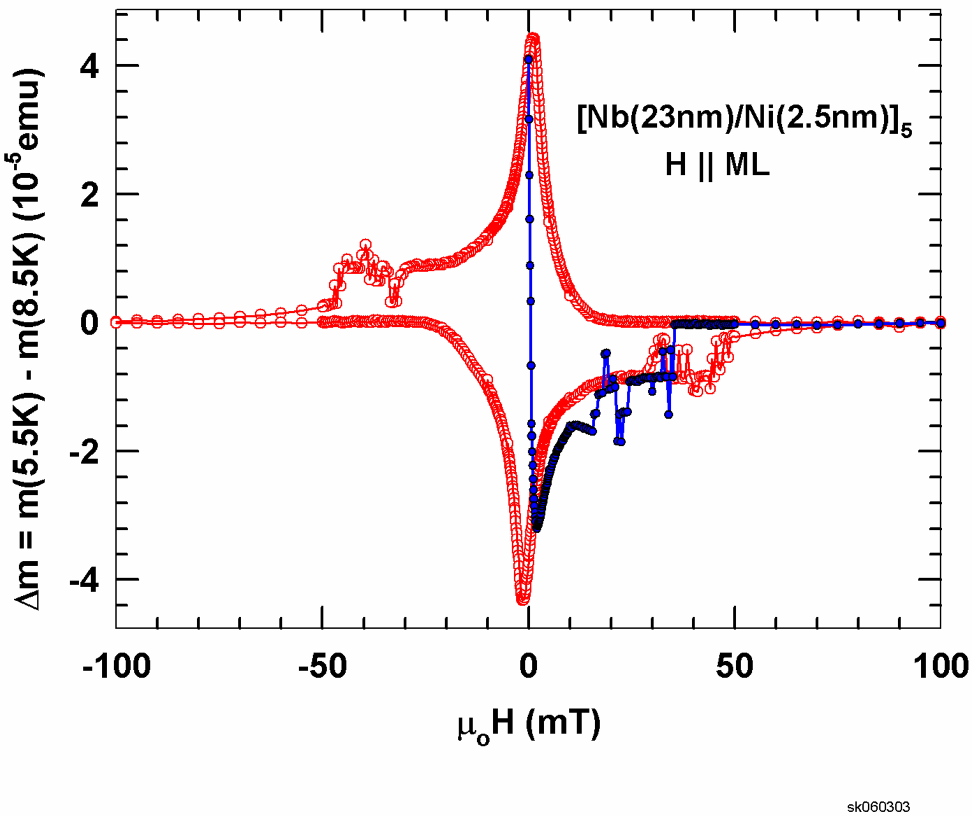

Fig. 7b De Long et al.

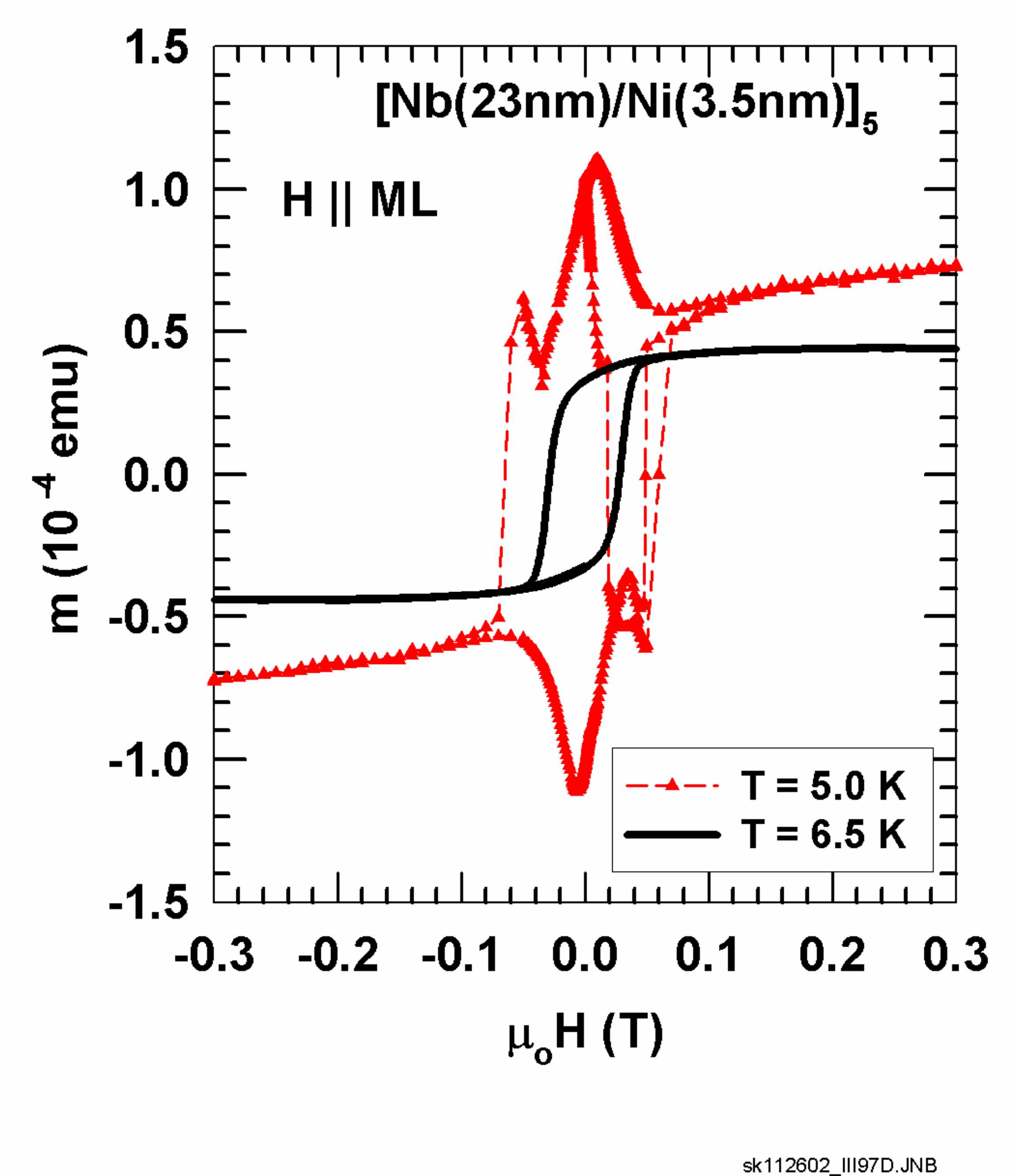

Fig. 8 De Long et al.

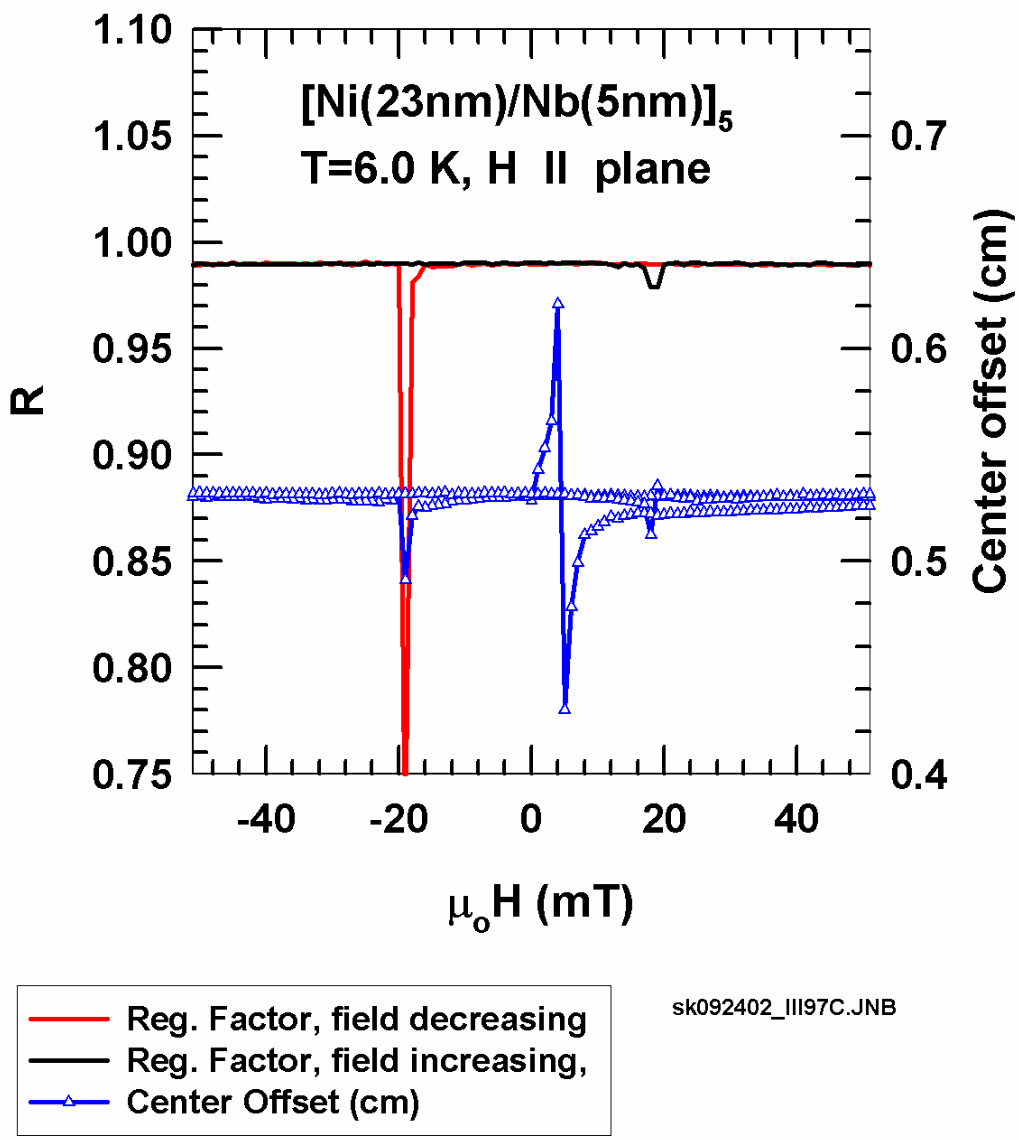

Fig. 9 De Long et al.

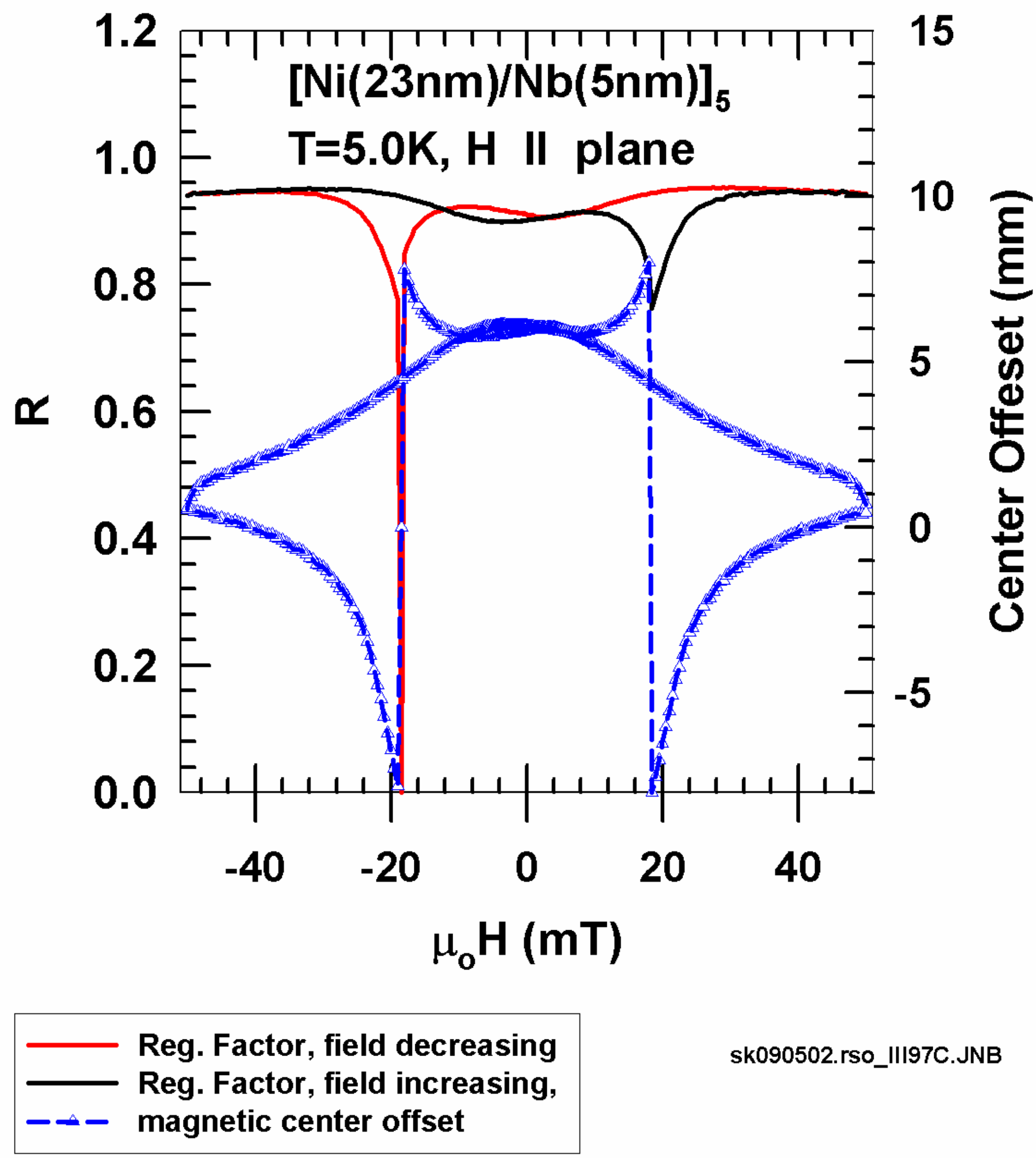

Fig. 10 De Long et al.

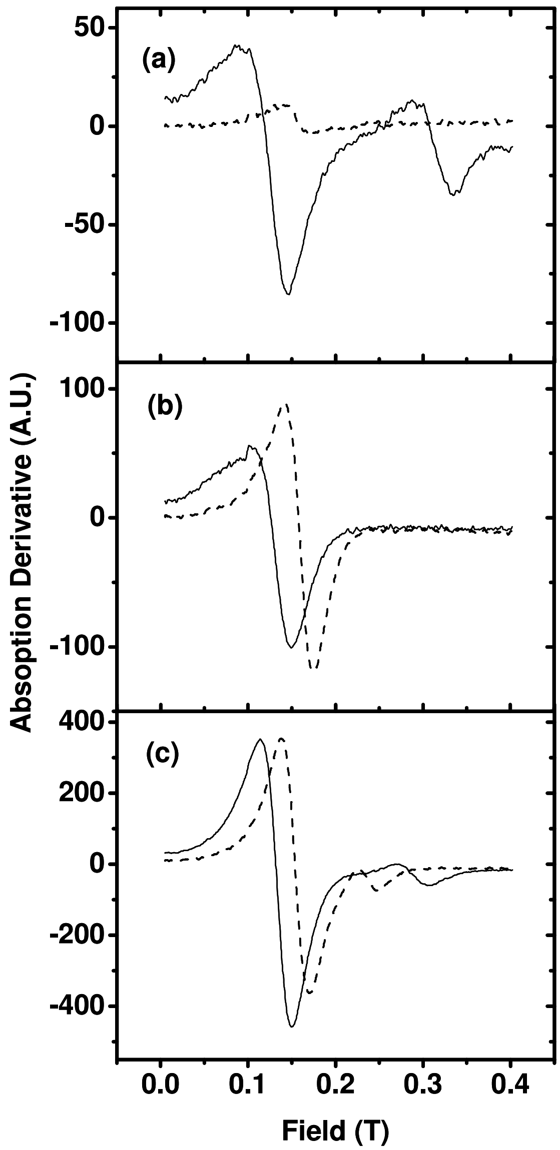

Fig. 11 De Long et al.

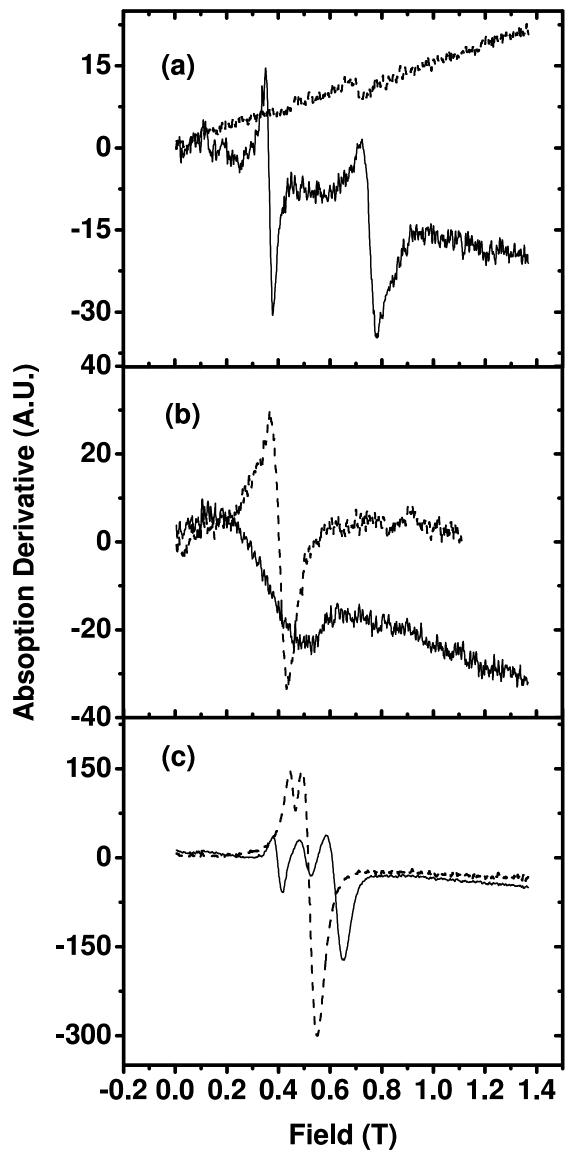

Fig. 12 De Long et al.

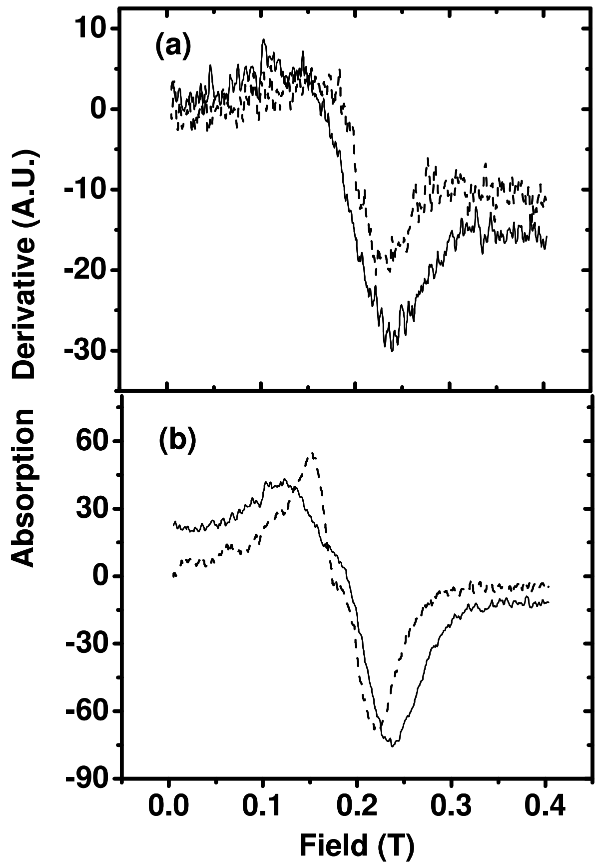

Fig. 13 De Long et al.

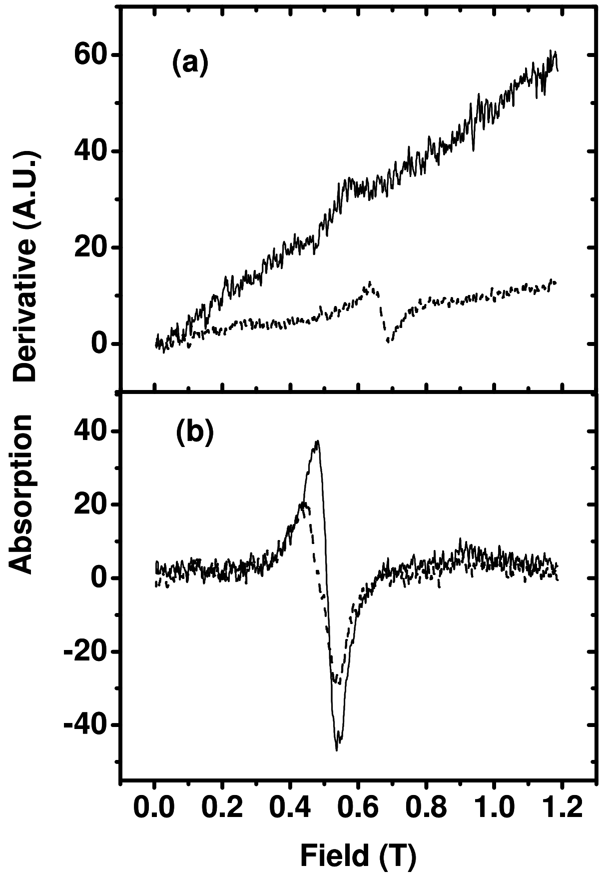

Fig. 14 De Long et al.